

Hybrid Tracking Control for Spark–Ignition Engines.*

Andrea Balluchi[†] Antonio Bicchi[‡] Canio Caterini[‡]
C. Rossi[§] A. Sangiovanni–Vincentelli^{†¶}

[†] PARADES G.E.I.E., Via San Pantaleo, 66, 00186 Roma, Italy,
balluchi, alberto@parades.rm.cnr.it

[‡] Centro Interdipartimentale di Ricerca “Enrico Piaggio”,
Università di Pisa, 56100 Pisa, Italy, bicchi@ing.unipi.it

[§] Magneti Marelli S.p.A., Via del Timavo, 33, 40134 Bologna, Italy, Carlo.Rossi@bologna.marelli.it

[¶] Dep. of Electrical Engineering and Computer Science,
University of California at Berkeley, CA 94720, alberto@eecs.berkeley.edu

Abstract

The design a hybrid feedback control for a spark ignition engine, equipped with an electronic–throttle valve, which achieves torque tracking is developed. The desired torque is supposed to be available on–line by interpreting the motion of the accelerator pedal that is actuated by the driver. A hybrid model that describes the interacting behavior of the intake manifold, the engine, the power–train and the catalytic converter is illustrated. The solution is obtained by decoupling the control problem into two subproblems: the intake manifold dynamics control and the torque generation process control (which includes catalytic converter management). The quality of the control law when applied to the hybrid model has been analytically demonstrated and a set of simulations are presented.

1 Introduction

In this paper, we focus on an application domain for hybrid system theory that is of great industrial interest: automotive engine control. The engine control problem is very complex (see e.g. [17, 24]). Figure 1 shows the decomposition of the system in a chain of its basic processes [3, 31, 50]. Air intake and fuel injection can be controlled to yield the desired mix to deliver to the combustion process. The timing of the sparks generated by the spark plugs determines the start of the combustion process that takes place in the cylinders. The torque and the emissions generated by the combustion process depend on the fuel mix (quantity of fuel and its dynamics) and on the spark ignition timing. The torque is then delivered to the power–train and the emissions to the exhaust subsystem. The goals for the control strategy are, in general, given in terms of emissions and torque but it is often the case that sub–goals are given by car manufacturers on all the processes in the chain.

¹This research has been partially sponsored by PARADES, a Cadence, Magneti-Marelli and SGS-Thomson GEIE, and by CNR.

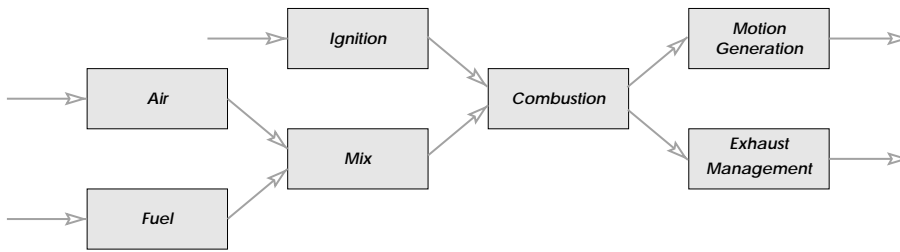


Figure 1: Functional decomposition of the system.

The literature on engine control is very rich. Most of the published works on control synthesis are based on average-value models (e.g. [31, 26, 17, 15, 52]) of the engine and the power-train and are devoted to the control of a particular phenomenon or subsystem during a particular operating condition. Cycle-accurate models are instead mainly used to analyze the behavior of the engine and in the design of mechanical parts, sensors and actuators ([44, 6, 47]), but they are scarcely used to design control laws (see e.g. [49]). Typical engine control problems are: the idle control ([33, 13, 1]), the air/fuel ratio control ([14, 42, 38]), the knocking and misfiring control ([23, 19]), the driveline oscillation control ([46, 9]).

We argue that the increasing requirements on the engine and power-train behavior both in terms of vehicle performance and tailpipe emissions as well as gas consumption, can be achieved only by using more accurate models than the ones proposed so far. An accurate model of a four-stroke gasoline engine has a “natural” hybrid representation because

- pistons have four modes of operation corresponding to the stroke they are in. Hence their behavior can be represented with a finite state model;
- power-train and air dynamics are continuous-time processes.

In addition, these processes interact tightly. In fact, the timing of the transitions between two phases of the pistons is determined by the continuous motion of the power-train, which, in turn, depends on the torque produced by each piston.

In our approach, the adoption of a hybrid formalism allows us to represent the cyclic behavior of the engine, thus capturing the effect of each fuel injection on the generated torque, the interaction between the discrete torque generation and the continuous power-train and air dynamics.

Hybrid systems have been the subject of intensive study in the past few years by both the control and the computer-science communities. Particular emphasis has been placed on a unified representation of hybrid models rooted in rigorous mathematical foundations ([22, 5, 2, 40, 29, 4, 30]). Some classical problems such as reachability analysis ([43, 18]), stability and safety ([35, 11, 39]) have been investigated and tools for their solutions, i.e. HyTech ([28, 27]), Kronos ([41]), Checkmate ([16]), developed.

In this paper, the problem of designing a feedback control which achieves engine torque tracking of a reference signal is addressed. The desired torque is available on-line by interpreting the motion of the accelerator pedal that is actuated by the driver.

The solution is obtained by decoupling the control problem in two subproblems: the first defined for the intake manifold dynamics (implemented by an inner control loop), the second

defined for torque generation process (implemented by an outer control loop).

The solution of the torque–tracking control problem is subject to constraints on the amount of non–stoichiometric mixed which can be supplied to the engine without saturating the catalytic converter storage mechanism. A remarkable point addressed in the proposed solution is that the best strategy of distribution of the control action, between fuel injection and air loading, to achieve both torque tracking and proper catalytic converter management is obtained.

Further, by means of a deep analysis of the closed–loop system the robustness properties of the proposed control have been analytically identified for the hybrid model of the engine. Indeed, the use of a hybrid framework, where discrete and continuous signals are modeled in a separate but integrated manner, is a definite advantage over other approaches, which approximate the system by converting it to continuous or discrete representations, thus obtaining solutions whose properties are not guaranteed.

The paper is organized as follows. In Section 2, we describe in detail a hybrid model of the engine, the power–train and the catalytic converter. In Section 3, we propose a hybrid torque–tracking control feedback for the engine, which is composed of two nested control loop: the inner for intake manifold control, and outer for torque generation. In Section 4, the behavior of the closed–loop hybrid system is analyzed and sufficient conditions, which guarantee convergence, torque tracking and proper catalytic converter management, are provided. Finally, in Section 5 the effectiveness of the proposed hybrid feedback is illustrated by discussing some interesting simulations.

2 Hybrid model of the engine

In this section, we review the model of a power–train equipped with an N –cylinder 4–stroke engine proposed in [7], which is here augmented to include the catalytic converter. The power–train hybrid model is described in the tagged–signal model (TSM) formalism proposed by Lee and Sangiovanni–Vincentelli [36, 37]. Such formalism allows us to formally describe systems represented as interacting processes of heterogeneous models of computation. In particular, we use a combination of FSMs, DESs and CTSs to form a hybrid system that is the basis for our design.

The overall system is composed of four main interacting blocks, namely the *intake manifold*, the *cylinders*, the *catalytic converter* and the *power–train* (Figure 2). The intake manifold pressure p is controlled by the throttle valve, which is powered by an electrical motor. We denote by v and α the motor input voltage and the throttle–valve position, respectively. The mass of air loaded in the cylinders depends on the pressure p and on the crankshaft revolution speed n .

The torque T produced by the engine is given by $\sum_{i=1}^N T^i$, where T^i is the torque generated by the i –th cylinder, which is determined by the mass of loaded air m^i , the mass of fuel q^i injected in the cylinder, and the *spark* ^{i} ignition command². The timing sequence of the four strokes of each cylinder is determined by the continuous motion of the crankshaft. We denote by θ the crankshaft angular position, which is obtained by the integration of the crankshaft velocity n .

²From this point on, we use the superscript i to indicate variables related to the i –th cylinder.

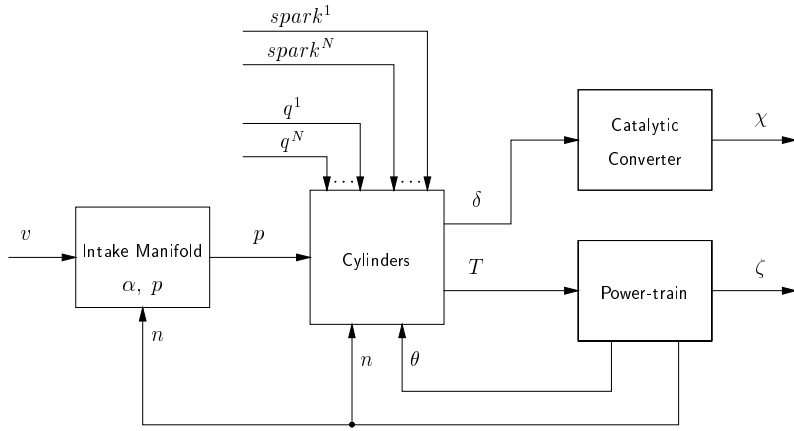


Figure 2: The engine blocks and their communication topology.

The generated torque T feeds the power-train dynamics whose state, denoted by ζ , contains the crankshaft revolution speed n and angle θ . To reduce tailpipe emissions χ , the exhausted gas δ is treated by the catalytic converter that, under suitable engine feedback control, guarantees emissions which meet the imposed standard.

2.1 The intake manifold.

Manifold pressure dynamics is a continuous-time process controlled by the throttle-valve position α that changes the effective section of the intake rail of the manifold. While in traditional engines the throttle valve is directly connected to the gas pedal, modern cars are equipped with an electronic-throttle system that allows full control of the intake manifold dynamics. Denoting by p the mean-value pressure and by v the electric motor input voltage, manifold dynamics is modeled as (see [10, 25]):

$$\dot{\alpha}(t) = a_{\alpha}\alpha(t) + b_{\alpha}v(t) \quad (1)$$

$$\dot{p}(t) = a_p p(t) + b_p \alpha(t) \quad (2)$$

Parameters a_p and b_p depend in on the geometric characteristics of the manifold, on the physical characteristics of the gas and atmosphere, and on the current value of the pressure p and engine speed n . In (1–2), we assume that an inner intake manifold control loop linearizes the intake manifold dynamics and compensates its dependency on the crankshaft speed n , so that a_p and b_p can be considered constant. The throttle angle and electric motor voltage are bounded as

$$\alpha \in [0, 90] \quad (3)$$

$$v \in [-V, +V] . \quad (4)$$

2.2 The cylinder.

The cylinder model is the most complex. It is “responsible” for torque generation. The torque T^i generated by each piston at each cycle depends on the thermodynamics of the air-fuel

mixture combustion process. The profile of T^i depends on the phases of the cylinder, the piston position ϕ^i , the mass m^i of air, the mass q^i of fuel both loaded in the cylinder during the intake phase, and on the spark ignition timing.

In a 4-stroke combustion engine, a piston reaches the *Top Dead Center* (TDC) (*Bottom Dead Center* (BDC)) when it is at its uppermost (lowermost) position. Each cylinder cycles through the following four phases:

- *intake* (I). The piston goes down from the TDC to the BDC loading the air–fuel mix present in the intake manifold;
- *compression* (C). The trapped mix is compressed by the piston during its upward movement from the BDC to the TDC;
- *expansion* (E). The combustion takes place pushing down the piston from the TDC to the BDC;
- *exhaust* (H). During its upward movement, from the BDC to the TDC, the piston expels combustion exhaust gases.

Let ϕ^i be the position of the i -th piston, expressed in terms of the corresponding crank angle, with respect to the last *Dead Center* (DC), that is

$$\phi^i(t) = [\theta(t) - \phi_0^i] \bmod 180^\circ, \quad (5)$$

where ϕ_0^i is the value of θ for which the i -th cylinder is at a DC. This corresponds to reset ϕ^i at the beginning of each phase. Note that since the pistons are connected to the crankshaft their positions ϕ^i are related to each other.

The quantity m^i of air loaded into each cylinder at the end of the intake run depends, in a nonlinear fashion, on the evolution of the intake manifold pressure and the crankshaft speed. The amount of air loaded up to time t , denoted by $m^i(t)$, is sampled at the intake BDC time t_ℓ to obtain the loaded air for the current engine cycle.

To achieve a proper combustion of the air-fuel mix, the amount of fuel q^i that can be injected into a cylinder is subject to constraints [48]. These constraints are usually expressed in terms of the air-to-fuel ratio $A/F = \frac{m^i}{q^i}$ of the mixture. When $A/F = (A/F)_{stoic} = 14.64$, the mix is said to be at stoichiometry, which is a desirable operating point for emissions. Rich mixtures $A/F < 14.64$ produce excess of CO and $H C$, while lean mixtures $A/F > 14.64$ have excess of NO_x . We denote by γ the equivalence ratio

$$\gamma(k) = \frac{(A/F)_{stoic}}{A/F} = (A/F)_{stoic} \frac{m^i(k)}{q^i(k)} \quad (6)$$

so that $\gamma = 1$ for stoichiometric mixture and $\gamma = 0$ when fuel is not injected. The allowed values of mixture composition are bounded by

$$\gamma(k) = [\gamma_{min}, \gamma_{max}] \cup \{0\} . \quad (7)$$

Spark ignition must occur at every cycle. Intuitively, it should occur exactly when the piston reaches the TDC of the compression stroke. Since the combustion process takes non-zero time

to complete, the pressure in the cylinder reaches its maximum some time after spark ignition. It is then convenient to produce a spark before the piston completes the compression stroke (*positive spark advance*), to achieve maximum fuel efficiency. Producing a spark after the piston has completed the compression phase and is in the expansion stroke (*negative spark advance*) may be used to reduce drastically the value of the torque generated during the expansion run. Hence, the spark control input has a very short delay and can be used to reduce torque much faster than using only the throttle valve. The spark ignition time is commonly defined in terms of the spark advance φ^i , which denotes the difference between the angle of the crank at the TDC between compression and expansion and the one at the time of ignition t_j^i . In terms of the piston position ϕ^i , we have

$$\varphi^i = \begin{cases} 180^\circ - \phi^i(t_j^i) & \text{for a positive spark advance} \\ -\phi^i(t_j^i) & \text{for a negative spark advance .} \end{cases} \quad (8)$$

Note that the spark advance has to be bounded both from above and from below to prevent the mix from not burning uniformly thus causing undesired knocking [21, 34] (upper bound) and from misfiring [19, 51] (lower bound), which causes undesired pollutants. These bounds depend on the revolution speed n . The spark advance and the amount of injected fuel is set at each cycle to control the generated torque (see [8]).

The air-fuel mixture is loaded in the cylinder during the intake stroke while the torque generation starts after the spark is ignited. Hence, to complete the description of the torque generation process, we need to model the delay between the time at which the mixture is loaded and the time at which the corresponding active torque is generated [32].

The overall model of the torque generation process for a single cylinder consists of four communicating processes of different MOCs:

- an FSM, modeling the 4-stroke engine cycle,
- a DES, modeling the discrete delay on the active torque generation, and
- two memory-less CTSs, modeling the air intake process and the profile of the generated torque.

Modeling the 4-stroke engine cycle with an FSM This part of the cylinder model is used to capture the sequential nature of the behavior of the cylinders. Based on the events generated by the spark ignition signal and by the reaching of dead centers, the FSM takes a transition and outputs the appropriate information to coordinate the other parts.

The four phases of the piston are associated to the states of an FSM that represents the behavior of the cylinder. A state transition would then occur when the piston reaches a dead center. However, the torque generated by the piston is related not only to the four phases of the piston but also to the spark generation process. Since spark ignition may occur either during the compression stroke or during the expansion stroke, a six state FSM is needed to model the possible behaviors of the cylinder. The cylinder FSM is shown in Figure 3. The FSM state s_k^i takes one of the following values

- I , denoting *Intake*.

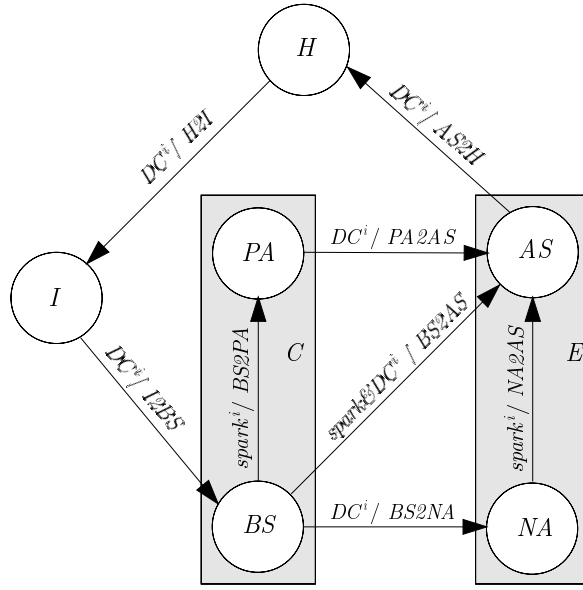


Figure 3: FSM describing the behavior of the i -th cylinder.

- BS , denoting *Before Spark*. The piston is in the compression stroke and no spark has been ignited yet.
- PA , denoting *Positive Advance*. The piston is in the compression stroke and the spark has been ignited.
- NA , denoting *Negative Advance*. The piston is in the expansion stroke and the spark has not been ignited yet.
- AS , denoting *After Spark*. The piston is in the expansion stroke and the spark has been ignited.
- H , denoting *Exhaust*.

The cylinder changes phase either when a spark is given (FSM input event $u_k^i = spark^i$ or $u_k^i = spark\&DC^i$ if the spark is given exactly at the dead center), or when a dead center is reached (FSM input event $u_k^i = DC^i$). The evolution of the torque produced by the cylinder depends on the transitions of the FSM, provided by the output o_k^i of the FSM that takes the following values: $BS2AS$, $BS2PA$, $BS2NA$, $PA2AS$, $NA2AS$, $AS2H$, $H2I$ and $I2BS$. The next-state and output functions of the cylinder FSM

$$s_{k+1}^i = \Lambda(s_k^i, u_k^i), \quad o_k^i = \Omega(s_k^i, u_k^i) \quad (9)$$

are shown in Figure 3. Note that, for the sake of notational simplicity, we dropped the superscript i , indicating the correspondence of the variable with cylinder i , from the index k .

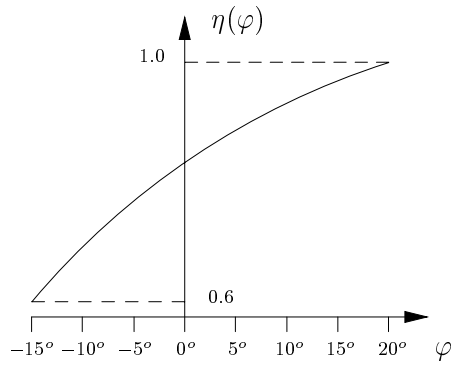


Figure 4: Ignition efficiency function (at low engine speed).

Modeling the air-intake process with a CTS Assuming small variations of the crankshaft speed n during intake and recalling that p represents the pressure mean-value over the engine cycle, a CTS linear model for the air intake can be used:

$$m^i(t) = c_p p(t) . \quad (10)$$

Modeling the torque profile with a CTS The profile of the torque T^i produced by the i -th piston can be expressed in terms of the motion of the piston given by ϕ^i (e.g. [49]). We set to zero the torque T^i during the passive phases of the cylinder, but we take into account the loss of energy due to these phases by reducing the amount of torque generated during the active phase. As a consequence of this simplification, the profile T^i is a piece-wise constant signal zero everywhere except in the expansion phase when the spark ignition command has already been given

$$T^i(t) = \begin{cases} G q^i \eta(\varphi^i) & \text{if } o_k \in \{PA2AS, BS2AS, NA2AS\} \\ 0 & \text{otherwise} \end{cases} \quad (11)$$

where: o_k^i is the current FSM output, the gain G represents the potential value of the torque that can be achieved by the given mix, and the ignition efficiency function $\eta(\varphi)$ has in general the profile shown in Figure 4.

Modeling the discrete delay on active torque generation with a DES The delay on active torque generation, which is characteristic of 4-stroke engine cycles, is modeled by means of a DES synchronized with the FSM transitions and whose dynamics depends on the FSM transitions:

$$\begin{aligned} z(k+1)^i &= f_{o_k^i}(z^i(k), v^i(k)) \\ y^i(k) &= h_{o_k^i}(z^i(k), v^i(k)) \end{aligned} \quad (12)$$

where o_k^i denotes the k -th FSM transition. The components of the DES input vector $v^i(k)$ are

- the mass of air m^i loaded during the intake phase;
- the mass of injected fuel q^i during the intake phase.

- the piston position ϕ^i , used to compute the spark advance φ^i according to (8);

The DES state $z^i(k)$ is used to model the delay between the mixture intake and the active torque generation. The DES output $y^i(k) = (m^i, q^i, \varphi^i, \delta^i)$ provides

- at the *NA2AS*, *BS2AS* and *PA2AS* transitions, the values (m^i, q^i, φ^i) to the CTS describing the profile of the engine torque (11);
- at the *AS2H* transition, the value δ^i of the unbalanced mixture mass, which will reach the catalytic converter, resulting from the combustion of q^i fuel with m^i air, i.e. $\delta^i = m^i - (A/F)_{stoic}q^i$.

The functions $f_{o_k^i}$ and $h_{o_k^i}$ describing the dynamics and the output of the DES are the following:

$$\begin{aligned}
f_{I2BS} &= (m^i(k), q^i(k), 0) \\
f_{BS2PA} &= z^i(k) + (0, 0, 180^\circ - \phi^i(k)) \\
f_{NA2AS} &= z^i(k) + (0, 0, -\phi^i(k)) \\
f_{o_k} &= z^i(k) \quad \text{for } o_k \in \{BS2NA, BS2AS, PA2AS, AS2H, H2I\}
\end{aligned} \tag{13}$$

$$\begin{aligned}
h_{BS2AS} &= h_{PA2AS} = (z^i(k), 0) \\
h_{NA2AS} &= (z^i(k), 0) + (0, 0, -\phi^i(k), 0) \\
h_{AS2H} &= (0, 0, 0, (z^i(k))_1 - (A/F)_{stoic}(z^i(k))_2) \\
h_{o_k} &= (0, 0, 0, 0) \quad \text{for } o_k \in \{BS2NA, I2BS, BS2PA, , H2I\}
\end{aligned} \tag{14}$$

Consider for example the torque produced in the state *AS* when a positive spark advance has been applied. According to the DES dynamics (13–14) this torque depends on the value of the DES output $y^i(k)$ at the transition *PA* \rightarrow *AS*, which in turn depends on values $m^i(k-2), q^i(k-2)$ at the transition *I* \rightarrow *BS*, i.e.:

$$\begin{aligned}
y^i(k) &= (z^i(k), 0) = ((z^i(k-1) + (0, 0, 180^\circ - \phi^i(k-1))), 0) \\
&= (m^i(k-2), q^i(k-2), 180^\circ - \phi^i(k-1), 0).
\end{aligned}$$

This shows how the DES model captures the delays in the torque generation process: a one-step delay associated to the spark ignition (due to the fact that the spark is given during the compression stroke while the torque is generated during the expansion stroke), and a two-step delay associated to the mix mass (due to the fact that the mix is loaded during the intake phase). Further, the unbalanced mixture mass δ^i , output at the *AS* \rightarrow *H* transition, is

$$\begin{aligned}
y^i(k) &= (0, 0, 0, (z^i(k))_1 - (A/F)_{stoic}(z^i(k))_2) = (0, 0, 0, (z^i(k-1))_1 - (A/F)_{stoic}(z^i(k-1))_2) \\
&= (0, 0, 0, (z^i(k-2))_1 - (A/F)_{stoic}(z^i(k-2))_2) = (0, 0, 0, m^i(k-3) - (A/F)_{stoic}q^i(k-3))
\end{aligned}$$

which shows how the three-step delay between air–fuel mixture intake and exhaust gas delivery is captured by the DES model.

2.3 The catalytic converter.

A three-way catalytic converter is commonly used in the exhaust system to reduce tailpipe emissions, in order to meet the standards imposed by government. The conversion efficiency of the converter is strongly related to the catalyst brick temperature [20]. For this reason a warm-up phase is necessary to fastly increase the converter temperature during a cold engine start up. We assume that the catalytic converter temperature is greater than the minimum light-off temperature (around 250°), so that the catalytic works at the maximum efficiency.

The functioning principle of a three-way catalytic converter is based on the oxygen storage and release mechanism. The conversion efficiency drastically decreases when such mechanism reaches a saturation point due to either excess of NO_x or HC and CO in the engine-out gas. A detailed model of a three-way catalytic convert is very complex since it comprises a description of the reaction kinetics, the exchanges between the reacting species and the surface of the catalyst, the thermodynamics and the gas dynamics. Our main concern in devising a solution to the force tracking control problem is to keep the catalytic converter far from saturation. Hence, we are interested in modeling the closeness of the catalytic converter to the saturation points. The capability of storing the oxygen depends on the equivalence ratio γ of the mixture. Indeed, assuming that at start up the catalytic converter is balanced, when the air-fuel mixture loaded by the cylinders is at stoichiometry, i.e. $\gamma = 1$, the oxygen storage and release mechanism of the catalytic converter remains balanced. Engine outputs of lean mixtures ($\gamma < 1$) and rich mixtures ($\gamma > 1$) unbalance the converter towards excess and lackness of oxygen, respectively.

The four component of the output y^i of the DES (13–14) modeling the cylinder behavior provides, at the $AS \rightarrow H$ cylinder FSM transition, the value of the unbalanced mixture mass $\delta^i = m^i - (A/F)_{stoic}q^i$ related to the current engine cycle. Such mass will feed the oxygen storage and release mechanism of the catalytic converter after some time due to the transport delay associated to the motion inside the pipe from the exhaust manifold to the catalytic converter. Hence, in order to control the state of storage of the catalytic converter it is sufficient to control the evolution of the sequence of unbalanced mixture masses $\delta^i(k)$. Indeed, the saturation constraints of the oxygen storage and release mechanism of the catalytic converter can be mapped ahead at the beginning of the exhaust pipe. By doing this we obtain a simplification of the model since it does not take into account of the exhaust pipe transport delay.

To model the storage mechanism at the beginning of the exhaust pipe a DES is used. The DES state variable l represents the unbalancement of the mixture masses in the engine-out gas delivered up to the current time. The DES systems, which receives from all cylinders the unbalanced mixture mass $\delta^i(k^i)$ given by (14), is as follows

$$l(k^0 + 1) = l(k^0) + \sum_{i=1}^N \delta^i(k^i) \quad (15)$$

where the sequence $\{t_{k^0}\}$ of times t_{k^0} at which (15) is updated is defined as $\cup_{i=1}^N \{t_{k^i}\}$, where $\{t_{k^i}\}$ denotes the sequence of times t_{k^i} at which the i -th cylinder DES (13–14) makes a step.

To prevent the catalytic converter from reaching a saturation point, the state l is bounded to satisfy the following constraint

$$l_h \in [l_{min}, l_{max}] \quad (16)$$

Dynamics (15) captures the storing nature of the catalytic converter: the unbalanced quantity of exhausted gas are trapped into the converter to be processed in the future. In (15) we assume a

linear dependency of l from the air and fuel masses. A refinement of this model can be obtained by using a nonlinear input map $\Psi(m^i, q^i)$, which should satisfy $\Psi(m^i, (A/F)_{stoic}m^i) = 0$.

2.4 The power–train.

In the force tracking control problem we assume that the clutch is engaged and a particular gear is selected. The power-train is described by the continuous time system

$$\dot{\zeta}(t) = A\zeta(t) + bT(t) - b_0 \quad (17)$$

$$\dot{\theta}(t) = (0, 6, 0)\zeta(t) \quad (18)$$

where $\zeta = (\alpha_e, n, \omega_p)^T$ includes the drive-line torsion angle, the crankshaft revolution speed, and the wheel revolution speed and θ is the crankshaft angle position. Input T is the torque produced by the engine. Vector b_0 models the resistant actions on the power–train, due to internal friction and external forces at the equilibrium point. Being the description of a passive system, dynamics (17) is exponentially stable and is characterized by a real dominant pole λ_1 , and a pair of conjugate complex poles $\lambda \pm j\mu$. Model parameters depend on the selected gear.

2.5 The power–train model for a 4–cylinder engine.

In this section the general power–train model introduced above is specialized to the case of a 4–cylinder in–line engine.

To take into account of the delay of spark ignition actuation, in the specification the control problem we require the value of the spark advance to be set at the intake BDC, that is at $I \rightarrow BS$ cylinder FSM transition. We denote by $r(k)$ the desired spark advance efficiency applied to the cylinder which takes the $I \rightarrow BS$ transition at time t_k . Assuming no noise on the spark actuation, $r(k)$ corresponds to the value of spark advance efficiency $\eta(\varphi)$ actually applied in the chosen cylinder for the current engine cycle. This allows us to simplify the cylinder FSM from 6 to 4 states.

Moreover, note that in 4–cylinder in–line engines, the cylinders are driven in such a way that at each instant of time each cylinder is in a different stroke of the engine cycle. Thanks to this symmetry the engine model can be drastically compacted. Indeed, the FSM can be reduced to a single–state FSM with a self–loop transition occurring at each dead center. The piston positions are identified by a unique variable $\phi(t) = \theta(t) \bmod 180^\circ$ given by (5).

To handle more easily the constraint (7) on fuel injection, we adopt an input transformation and consider γ^i as the injection input in place of q^i . Further, fuel injection actuation is modeled by a discrete delay of one transition in the cylinder DE dynamics. The produced torque is then expressed as $T(k) = G c_p \gamma(k-1) p(t_{k-2}) r(k-1)$, where $\gamma(k)$ denotes the value of equivalence ratio for the cylinder which takes the $H \rightarrow I$ transition. Considering γ^i the injection input, the unbalanced mixture mass δ^i is rewritten as: $\delta^i = m^i - (A/F)_{stoic}q^i = (1 - \gamma^i)m^i = (1 - \gamma^i)c_p p$. We denote by $\delta(k)$ the unbalanced mixture mass of the cylinder which takes the $AS \rightarrow H$ transition at time t_k .

Since the cylinder FSM is reduced to a single-state FSM, the catalytic converter dynamics (15) evolves on the unique sequence of transition times $\{t_k\}$, corresponding to the piston dead centers, and receives as input the variable $\delta(k)$.

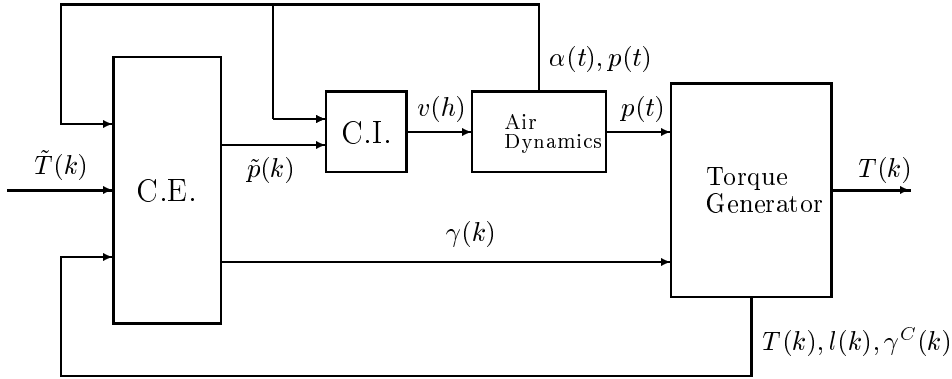


Figure 5: Decentralized control loops scheme.

The hybrid model of the power-train with 4-cylinder in-line engine, is composed of the following interacting components:

1. a CTS as in (1–2), modeling the throttle valve and intake manifold dynamics which are subject to the constraints (4) and (3);
2. a single-state FSM, which generates the dead center events from the piston evolution $\phi(t)$ taking a self-loop transition;
3. a DES, active at each FSM transition and modeling the torque generation and catalytic converter dynamics. By (11), (10), (13–14) and (15) we have

$$\gamma^C(k+1) = \gamma(k) \quad (19)$$

$$T(k+1) = G c_p \gamma^C(k) p(t_k) r(k) \quad (20)$$

$$\delta^E(k+1) = c_p (1 - \gamma^C(k)) p(t_k) \quad (21)$$

$$\delta(k+1) = \delta^E(k) \quad (22)$$

$$l(k+1) = l(k) + \delta(k) \quad (23)$$

where: $\gamma^C(k)$ is the equivalence ratio γ of the cylinder in the compression stroke, and $\delta^E(k)$ denotes the unbalance mixture mass of the cylinder that begins the expansion stroke. Dynamics (23) is subject to constraint (16).

4. a CTS as in (17–18), modeling the power-train mechanical dynamics.

3 Control design

Our approach to the torque-tracking control problem is to decouple the control problem by synthesizing two nested loop:

1. an *intake manifold control* — in the inner loop;

2. a torque generation control — in the outer loop.

The intake manifold control is designed by solving a minimum–time control problem with respect to a reference trajectory $\hat{p}(t)$, for the intake manifold pressure $p(t)$, which is a ramp–signal. The synthesis of this control is obtained in Section 3.1 by applying the Pontryagin Maximum Principle in the continuous–time domain [45].

The aim of the torque generation control is to find the best politic of distribution of the control action, between fuel injection and air loading, which achieves both torque tracking and proper catalytic converter management. The reference torque is assumed to be a ramp–signal and a quadratic cost function is used to measure tracking performance. The catalytic converter imposes constraints on the amount of non–stoichiometric mixed which can be supplied to the engine without saturating the catalytic converter storage mechanism. In Section 3.2, a solution to the torque generation control is derived in the discrete–time domain [12]. The feedback control is expressed in terms of: the equivalence ratio $\gamma(k)$ to be applied during fuel injection, and the desired value of manifold pressure $\tilde{p}(k)$ to be used by the intake manifold control loop.

In Section (3.3), a hybrid feedback control for the hybrid model of the engine described in Section 2 is derived from the two decouplingly designed control loops. The use of reference ramp–signals in both control loops allows us to

1. interface the outer and the inner control loops: at each dead center the torque generation control defines a ramp reference signal $\tilde{p}(t)$ to be tracked by the intake manifold pressure;
2. extend the feedback control to the case of tracking a reference torque signal $\hat{T}(t)$ of generic shape in time: at each dead center the given reference torque signal, provided on–line, is approximated by the current expression of the local tangent.

Finally, in Section 4, the behavior of the closed–loop hybrid system in approaching and tracking a generic reference torque signal is analyzed in depth and sufficient conditions, under which convergence and torque tracking as well as proper catalytic converter management are guaranteed, are provided.

3.1 Intake manifold control

The feedback control for the intake manifold dynamics (1–2) is designed by solving first a minimum–time tracking control problem with respect to a reference pressure trajectory which is ramp signal:

$$\hat{p}(t) = m_p t + n_p . \quad (24)$$

When $p(t)$ is forced to track the reference signal (24), we have $\dot{p}(t) = m_p$, which replaced into (1) gives the reference trajectory for the throttle angle and the throttle motor input:

$$\hat{\alpha}(t) = -\frac{a_p}{b_p} \hat{p}(t) + \frac{m_p}{b_p} = -\frac{a_p m_p}{b_p} t + \frac{m_p - a_p n_p}{b_p} = m_\alpha t + n_\alpha \quad (25)$$

$$v(t) = -\frac{a_\alpha}{b_\alpha} \hat{\alpha}(t) - \frac{a_p m_p}{b_p b_\alpha} . \quad (26)$$

where $m_\alpha = -\frac{a_p m_p}{b_p}$ and $n_\alpha = \frac{m_p - a_p n_p}{b_p}$. Further, the formalization of the optimal control problem for the time varying reference trajectory (24–25) is obtained by augmenting the state

space with a state variable β denoting the elapsed time. The minimum–time tracking control problem to solve is:

Problem 3.1.1 *Given an initial state $(\alpha, p, \beta) = (\alpha_0, p_0, 0)$,*

$$\min_{v(t)} \beta(t_f) \quad (27)$$

subject to the dynamics

$$\begin{aligned} \dot{\alpha}(t) &= a_\alpha \alpha(t) + b_\alpha v(t) \\ \dot{p}(t) &= b_p \alpha(t) + a_p p(t) \\ \dot{\beta}(t) &= 1 \end{aligned} \quad (28)$$

and the constraints

$$v(t) \in [-V, V] \quad (29)$$

$$(\alpha(t_f), p(t_f), \beta(t_f)) \in \mathcal{S} \quad (30)$$

where the target set is

$$\mathcal{S} \equiv \begin{cases} p - m_p \beta - n_p = 0 \\ \alpha - m_\alpha \beta - n_\alpha = 0 \end{cases} . \quad (31)$$

The Hamiltonian associated to the above minimum–time problem is

$$\begin{aligned} H(t) &= \pi_\alpha \dot{\alpha} + \pi_p \dot{p} + \pi_\beta \dot{\beta} + \nu_1(\alpha - 90) - \nu_2 \alpha \\ &= \pi_\alpha (a_\alpha \alpha + b_\alpha v) + \pi_p (a_p p + b_p \alpha) + \pi_\beta + \nu_1(\alpha - 90) - \nu_2 \alpha \end{aligned} \quad (32)$$

where ν_1 and ν_2 are the Lagrange multipliers corresponding to the state constraint (3), defined by

$$\begin{cases} \nu_1 = 0 & \text{if } \alpha < 90 \\ \nu_1 \geq 0 & \text{if } \alpha = 90 \end{cases} \quad \begin{cases} \nu_2 = 0 & \text{if } \alpha > 0 \\ \nu_2 \geq 0 & \text{if } \alpha = 0 \end{cases} .$$

The adjoint variables are subject to the dynamics

$$\begin{aligned} \dot{\pi}_\alpha(t) &= -\frac{\partial H}{\partial \alpha} = -a_\alpha \pi_\alpha - b_p \pi_p + \nu_1 - \nu_2 \\ \dot{\pi}_p(t) &= -\frac{\partial H}{\partial p} = -a_p \pi_p \\ \dot{\pi}_\beta(t) &= -\frac{\partial H}{\partial \beta} = 0 \end{aligned} \quad (33)$$

The transversality condition requires that at the final time t_f the adjoint vector $[\pi_\alpha, \pi_p, \pi_\beta]^T$ should lie on the subspace perpendicular to the target set \mathcal{S} as in (31). That is

$$m_\alpha \pi_\alpha(t_f) + m_p \pi_p(t_f) + \pi_\beta(t_f) = 0 . \quad (34)$$

The boundary conditions problem is defined by the extended dynamics (28) and (33), the initial condition $(\alpha, p, \beta) = (\alpha_0, p_0, 0)$, and the final conditions (34) and $(\alpha(t_f), p(t_f), \beta(t_f)) \in \mathcal{S}$ with \mathcal{S} as in (31).

If the constraints (3) are tight, then the integration of the adjoint dynamics gives

$$\pi_\alpha(t) = \left(\pi_\alpha(t_f) + \pi_p(t_f) \frac{b_p}{a_\alpha - a_p} \right) e^{-a_\alpha(t-t_f)} - \pi_p(t_f) \frac{b_p}{a_\alpha - a_p} e^{-a_p(t-t_f)} \quad (35)$$

$$\pi_p(t) = \pi_p(t_f) e^{-a_p(t-t_f)} \quad (36)$$

$$\pi_\beta(t) = \pi_\beta(t_f) \quad (37)$$

Hence, non-singular optimal controls are given by

$$v(t) = \begin{cases} +V & \text{if } b_\alpha \pi_\alpha(t) < 0 \\ -V & \text{if } b_\alpha \pi_\alpha(t) > 0 \end{cases} . \quad (38)$$

Solution (35) can be rewritten as

$$\pi_\alpha(t) = \left(\pi_\alpha(t_f) + \pi_p(t_f) \frac{b_p}{a_\alpha - a_p} \right) e^{(a_p - a_\alpha)(t-t_f)} - \pi_p(t_f) \frac{b_p}{a_\alpha - a_p} = 0 \quad (39)$$

from which one deduces that, along a non-singular optimal arc, $\pi_\alpha(t)$ can be zero at most once. The switching surface for the optimal control is obtained by backwards intergration of the extended dynamics (28) and (33) from a final condition with $(\alpha(t_f), p(t_f), \beta(t_f)) \in \mathcal{S}$. If, at some time $t = -\Delta + t_f$, we have $\pi_\alpha(-\Delta + t_f) = 0$ then a control switching takes place. When the control switching occurs the state (α, p, β) evaluates to

$$\begin{pmatrix} \alpha \\ p \\ \beta \end{pmatrix} = \begin{pmatrix} A_p(-\Delta) & 0 \\ 0 & 1 \end{pmatrix} \begin{pmatrix} \hat{\alpha}(t_f) \\ \hat{p}(t_f) \\ \beta(t_f) \end{pmatrix} + \begin{pmatrix} B_p(-\Delta)v \\ -\Delta \end{pmatrix} \quad (40)$$

where $v \in \{-V, V\}$ and

$$A_p(t) = \begin{pmatrix} e^{a_\alpha t} & 0 \\ \frac{b_p e^{(a_\alpha - a_p)t}}{a_\alpha - a_p} & e^{a_p t} \end{pmatrix} \quad \text{and} \quad B_p(t) = (I - A_p(t)) \begin{pmatrix} -\frac{b_\alpha}{a_\alpha} \\ \frac{b_p}{a_p} \frac{b_\alpha}{a_\alpha} \end{pmatrix} . \quad (41)$$

The two dimensional switching surface (40) is parametrized in terms of the final time t_f and the switching time Δ . By replacing (24) and (25) in (40), since $\beta(t) = \beta(t_f) - \Delta$, the surface (40) is mapped into the (α, p) subspace as follows:

$$\alpha = e^{-a_\alpha \Delta} \hat{\alpha} + (1 - e^{-a_\alpha \Delta}) \alpha_v \quad (42)$$

$$p = \frac{b_p}{a_\alpha - a_p} (e^{a_\alpha \Delta} - e^{a_p \Delta}) (\hat{\alpha} + \alpha_v) e^{-a_p \Delta} \hat{p} + (1 - e^{-a_p \Delta}) p_v . \quad (43)$$

where $(\alpha_v, p_v)^T = B_p(-\Delta)v$ with $B_p(\cdot)$ as in (41). Note that, since the system of equations (42–43) is lower triangular then the equation (42) can be solved for Δ given a value of α . Hence, to test whether or not a given state (α, p) belongs to the switching surface, the pressure p is compared to the right-hand side of (43) computed for the determined Δ . Given a point (α, p) , let Δ^* denote the solution to (42) and $p^*(\Delta)$ denote the right-hand side of (43) for a given Δ . Define the function $\sigma : \mathbb{R}^2 \rightarrow \mathbb{R}$ as:

$$\sigma(\alpha, p) = p - p^*(\Delta^*) . \quad (44)$$

The minimum–time control for non–singular trajectories is

$$v(t) = \begin{cases} +V & \text{if } (\sigma(\alpha, p) < 0) \vee ((\sigma(\alpha, p) = 0) \wedge (\alpha < \hat{\alpha})) \\ -V & \text{if } (\sigma(\alpha, p) > 0) \vee ((\sigma(\alpha, p) = 0) \wedge (\alpha > \hat{\alpha})) \end{cases} . \quad (45)$$

In minimum–time trajectories to the target set \mathcal{S} , singular arcs appear when the throttle angle α reaches one of the boundaries $\alpha = 0$ and $\alpha = 90$. In such case, either $\nu_1 \neq 0$ or $\nu_2 \neq 0$ and the optimal control is

$$v(t) = \begin{cases} -90 \frac{a_\alpha}{b_\alpha} & \text{if } \alpha(t) = 90 \\ 0 & \text{if } \alpha(t) = 0 \end{cases} . \quad (46)$$

The bang–bang control (45) is readily extended to obtain the minimum–time tracking control for trajectories which contain singular arcs. Indeed, singular arcs end when the state (α, p) reaches the switching surface $\sigma(\alpha, p) = 0$ with $\sigma(\alpha, p)$ as in (44). Furthermore, trajectories approaching a singular arc under a control v chosen according to (45) are optimal since this is the fastest way in which α can evolve.

In conclusion, from (26), (45) and (46), the minimum–time tracking control which is a solution to Problem 3.1.1 is

$$v(t) = \begin{cases} +V & \text{if } [(\sigma(\alpha, p) < 0) \vee ((\sigma(\alpha, p) = 0) \wedge (\alpha < \hat{\alpha}))] \wedge (\alpha < 90) \\ -90 \frac{a_\alpha}{b_\alpha} & \text{if } [(\sigma(\alpha, p) < 0) \vee ((\sigma(\alpha, p) = 0) \wedge (\alpha < \hat{\alpha}))] \wedge (\alpha = 90) \\ -V & \text{if } [(\sigma(\alpha, p) > 0) \vee ((\sigma(\alpha, p) = 0) \wedge (\alpha > \hat{\alpha}))] \wedge (\alpha > 0) \\ 0 & \text{if } [(\sigma(\alpha, p) > 0) \vee ((\sigma(\alpha, p) = 0) \wedge (\alpha > \hat{\alpha}))] \wedge (\alpha = 0) \\ -\frac{b_p a_\alpha \alpha + a_p m_p}{b_p b_\alpha} & \text{if } (\alpha = \hat{\alpha}) \wedge (p = \hat{p}) \end{cases} \quad (47)$$

3.2 Torque generation control

In this section, a feedback control that achieves tracking of a reference torque ramp signal \hat{T} for the torque generation process is devised. The torque generation model is obtained from the DES modeling the cylinder behavior presented Section 2.5. The reference torque profile is describe by the equation $\hat{T}(k+1) = \hat{T}(k) + m\tau$ where m and τ are constant, the latter indicating the time between two dead centers. The decoupling of the torque generation control with respect to the intake manifold control is based on an abstraction of the dynamics of the intake manifold closed–loop system, which is modeled by a simple one step delay system, $p(k+1) = \tilde{p}(k)$, whose input $\tilde{p}(k)$ denotes the desired manifold pressure. The spark advance efficiency is always set to the optimal value $r(k) = 1$ to reduce fuel consumption. The advantages of modulating the spark advance efficiency will be investigated in future work. Hence, the DES describing the torque generation process is completed by the delay equation on fuel injection actuation (19), the torque generation equation (20) and the catalytic converter equation (23). The delay equation (21) and (22) can be abstracted by considering the mixture unbalance at the intake phase instead of the exhaust phase. The input to the torque generation process are: the equivalence ratio $\gamma(k)$ and the desired manifold pressure $\tilde{p}(k)$.

The torque generation control problem is specified as follows

Problem 3.2.1 *Given an initial state $(\hat{T}(0), p(0), \gamma^C(0), T(0), l(0)) = (\hat{T}_0, p_0, \gamma_0^C, T_0, l_0)$*

$$\min_{\gamma(k), \tilde{p}(k)} \sum_{i=0}^{\infty} \frac{W}{2} (T(i) - \hat{T}(i))^2 \quad (48)$$

subject to the dynamics

$$\begin{aligned}
\hat{T}(k+1) &= \hat{T}(k) + m\tau \\
p(k+1) &= \tilde{p}(k) \\
\gamma^C(k+1) &= \gamma(k) \\
T(k+1) &= Gc_p p(k) \gamma^C(k) \\
l(k+1) &= l(k) + c_p (1 - \gamma^C(k)) p(k)
\end{aligned} \tag{49}$$

and the constraints

$$\gamma(k) \in [\gamma_{min}, \gamma_{max}] \tag{50}$$

$$\tilde{p}(k) \in [\tilde{p}_{min}, \tilde{p}_{max}] \tag{51}$$

$$l(k) \in [l_{min}, l_{max}] \tag{52}$$

$$\lim_{k \rightarrow \infty} l(k) = 0 \tag{53}$$

A solution to the optimal control Problem 3.2.1 is determined from the solution to a simplified optimal control problem obtained by relaxing the constraint on $l(k)$. When the dynamics of $l(k)$ are removed from (49), the state components p and z can be collapsed to a single component as well as the inputs $hatp$ and γ . The simplified optimal control problem is:

Problem 3.2.2 Given an initial state $(\hat{T}(0), z(0), T(0)) = (\hat{T}_0, z_0, T_0)$

$$\min_{u(k)} \sum_{i=0}^{\infty} \frac{W}{2} (T(i) - \hat{T}(i))^2 \tag{54}$$

subject to the dynamics

$$\begin{aligned}
\hat{T}(k+1) &= \hat{T}(k) + m\tau \\
z(k+1) &= u(k) \\
T(k+1) &= Gc_p z(k)
\end{aligned} \tag{55}$$

and the constraints

$$u(k) \in [u_{min}, u_{max}] \tag{56}$$

where $u_{max} = \tilde{p}_{max} \gamma_{max}$ and $u_{min} = \tilde{p}_{min} \gamma_{min}$.

The Hamiltonian associated to the above optimal control problem is:

$$\begin{aligned}
H(k) &= \frac{W}{2} (T(k) - \hat{T}(k))^2 + \lambda_r(k+1)u(k) + \lambda_s(k+1)Gc_p z(k) + \\
&\quad \lambda_{\hat{T}}(k+1)(\hat{T}(k) + m\tau + \nu_s(k)(u(k) - u_{max}) + \nu_i(k)(-u(k) + u_{min})).
\end{aligned} \tag{57}$$

where the Lagrange multipliers ν_s and ν_i are defined by

$$\begin{cases} \nu_i(k) = 0 & \text{if } u(k) > u_{min} \\ \nu_i(k) > 0 & \text{if } u(k) = u_{min} \\ \nu_s(k) = 0 & \text{if } u(k) > u_{max} \\ \nu_s(k) > 0 & \text{if } u(k) = u_{max} \end{cases} \tag{58}$$

and the adjoint variables λ_z , λ_s and $\lambda_{\hat{T}}$ are subject to the dynamics

$$\lambda_z(k) = \frac{\partial H(k)}{\partial r} = Gc_p \lambda_T(k+1) \quad (59)$$

$$\lambda_s(k) = \frac{\partial H(k)}{\partial s} = W(T(k) - \hat{T}(k)) \quad (60)$$

$$\lambda_{\hat{T}}(k) = \frac{\partial H(k)}{\partial \hat{T}} = \lambda_{\hat{T}}(k+1) - (W(T(k) - \hat{T}(k))) . \quad (61)$$

The boundary conditions are given on: the initial system state (\hat{T}_0, z_0, T_0) and the final adjoint state that has to be null. The optimal $u(k)$ is found by setting

$$\frac{\partial H}{\partial u} = GW(Gc_p u(k) - \hat{T}(k+2))c_p + \nu_s(k) - \nu_i(k) = 0 . \quad (62)$$

By (58), three cases are in order:

1. $u(k) \in (u_{min}, u_{max})$, since by (58) $\nu_i(k) = \nu_s(k) = 0$, then by (62) $u(k) = \frac{\hat{T}(k+2)}{Gc_p}$;
2. $u(k) = u_{max}$, by (58) $\nu_i(k) = 0$, $\nu_s(k) \geq 0$, and by (62) $\nu_s(k) = GW(Gc_p u_{max}(k) - \hat{T}(k+2))c_p \geq 0$;
3. $u(k) = u_{min}$, by (58) $\nu_s(k) = 0$, $\nu_i(k) \geq 0$, and by (62) $\nu_i(k) = -GW(Gc_p u_{min}(k) - \hat{T}(k+2))c_p \geq 0$.

Hence, a solution to the optimal control problem 3.2.2 is:

$$u(k) = sat \begin{cases} \tilde{p}_{max} \gamma_{max} \\ \frac{\hat{T}(k+2)}{Gc_p} \\ \tilde{p}_{min} \gamma_{min} \end{cases} . \quad (63)$$

The following holds:

Lemma 3.2.1 *Given $u(k)$, (63) yields if and only if for all $\gamma(k)$ and $\tilde{p}(k)$ such that $\gamma(k)\tilde{p}(k) = u(k)$ there exists $\bar{\gamma}(k) \in [\gamma_{min}, \gamma_{max}]$ such that*

$$\tilde{p}(k) = sat \begin{cases} \tilde{p}_{max} \\ \frac{\hat{T}(k+2)}{Gc_p \bar{\gamma}(k)} \\ \tilde{p}_{min} \end{cases} \quad \gamma(k) = sat \begin{cases} \gamma_{max} \\ \frac{\hat{T}(k+2)}{Gc_p \tilde{p}(k)} \\ \gamma_{min} \end{cases} \quad (64)$$

The proof of this Lemma is reported in appendix.

Lemma 3.2.1 allows us to express the solution (63) to Problem 3.2.2 in terms of the equivalence ratio $\gamma(k)$ and the desired manifold pressure $\tilde{p}(k)$ using (64). However, since the dynamics of l has been abstracted away in Problem 3.2.2, (64) has to be refined to take into account of the constraints (52) and (53) defined in Problem (3.2.1).

To enforce on the trajectories of system (49) the constraint (52), (64) is modified as follows:

$$\tilde{p}(k) = sat \begin{cases} \tilde{p}_{max} \\ \frac{\hat{T}(k+2)}{Gc_p \bar{\gamma}(k)} \\ \tilde{p}_{min} \end{cases} \quad \gamma(k) = sat \begin{cases} \hat{\gamma}_{max} \\ \frac{\hat{T}(k+2)}{Gc_p \tilde{p}(k)} \\ \hat{\gamma}_{min} \end{cases} \quad (65)$$

where $\bar{\gamma}(k) \in [\hat{\gamma}_{min}, \hat{\gamma}_{max}]$ and

$$\begin{aligned}\hat{\gamma}_{max} &= \min\left\{1 + \frac{l(k) + c_p p(k)(1 - \gamma^C(k)) - l_{min}}{c_p \tilde{p}(k)}, \gamma_{max}\right\} \\ \hat{\gamma}_{min} &= \max\left\{1 + \frac{l(k) + c_p p(k)(1 - \gamma^C(k)) - l_{max}}{c_p \tilde{p}(k)}, \gamma_{min}\right\}\end{aligned}\quad (66)$$

Further, by choosing among all the possible values for $\bar{\gamma}$,

$$\bar{\gamma}(k) = \text{sat} \begin{cases} \gamma_{max} \\ \frac{\hat{T}(k+2)}{\hat{T}(k+2) - QG(l(k) + c_p p(k)(1 - \gamma^C(k)))} \\ \gamma_{min} \end{cases}\quad (67)$$

with $Q \in (0, 1]$, constraint (53) is also satisfied as guaranteed by the following lemmas.

Lemma 3.2.2 *If*

$$\gamma_{max} \leq 1 - \frac{l_{min}}{c_p \tilde{p}_{max}} \quad \text{and} \quad \gamma_{min} \geq 1 - \frac{l_{max}}{c_p \tilde{p}_{min}},\quad (68)$$

*then*³ $\bar{\gamma}(k)$ as in (67) satisfies $\bar{\gamma}(k) \in [\hat{\gamma}_{min}, \hat{\gamma}_{max}]$.

Lemma 3.2.3 *If the reference signal $\hat{T}(k)$ is such that there exists a $\bar{k} > 0$ for which*

$$\hat{T}(k) \in (Gc_p \tilde{p}_{min}, Gc_p \tilde{p}_{max}) \quad \forall k > \bar{k},\quad (69)$$

*then*⁴ *under feedback (65), the sequence of $l(k)$ can be bounded as follows*

$$0 \leq (1 - Q)|l(k)| \leq |l(k+1)| < |l(k)| \quad \forall k > \bar{k} + 1.\quad (70)$$

The proofs of Lemmas 3.2.2 and 3.2.3 are reported in appendix.

By Lemma 3.2.3 convergence of $l(k)$ to zero is guaranteed for any $Q \in (0, 1]$. The velocity of convergence is upper bounded by $1 - Q$ and the fastest convergence is achieved for $Q = 1$.

3.3 Hybrid torque–tracking control

In this section a hybrid feedback control which solves the torque tracking problem for the hybrid model of the engine described in Section 2 is proposed. Such control is made of two nested loop: the inner one is derived from Section 3.1 and controls the intake manifold, while the outer one is derived from Section 3.2 and controls the torque generation.

³Under these constraints we have that for any $l(k) > 0$ ($l(k) < 0$) we cannot have $l(k+1) < l_{min}$ ($l(k+1) > l_{max}$ resp.), which is a reasonable assumption for the model of a commercial car.

⁴This is a very mild hypothesis since it requires that the plant should be able to track the reference signal \hat{T} with $\gamma \in (\gamma_{min}, \gamma_{max})$.

3.3.1 Inner loop: intake manifold control

Since the engine control unit is implemented by a digital system, in this section a discretized version of the intake manifold control developed in Section 3.1 is derived. Let τ_0 denote the sampling period of the discrete-time intake manifold control and let $\{t_h\}$ denote the sequence of sampling times. The period- τ_0 discrete-time model of the intake manifold is obtained from (1-2) as follows

$$\begin{pmatrix} \alpha(h+1) \\ p(h+1) \end{pmatrix} = A_p(\tau_0) \begin{pmatrix} \alpha(h) \\ p(h) \end{pmatrix} + B_p(\tau_0)v(h) \quad (71)$$

where $A_p(\tau_0)$ and $B_p(\tau_0)$ are as in (41).

The direct application of the continuous-time feedback control (47) to the discrete-time dynamics (71) would generate a chattering behavior around the point $(\hat{\alpha}, \hat{p})$. Hence, the bang-bang control (47) is adopted to steer the state of the intake manifold dynamics (71) to a nonzero measure set centered on $(\hat{\alpha}, \hat{p})$ of type

$$\mathcal{R}(\hat{\alpha}, \hat{p}) = \left\{ (\alpha, p) \in [0, 90] \times [0, \infty) : (\alpha - \hat{\alpha})^2 + (p - \hat{p})^2 \leq \rho_1^2 \wedge |\sigma(\alpha, p)| \leq \rho_2 \right\} \quad (72)$$

where $\sigma(\alpha, p)$ as in (44) measures the distance of the state (α, p) from the intake manifold optimal switching surface and ρ_1, ρ_2 are control parameters.

Let $x|_{(2)}$ denotes the second component of a given vector x . For any (α, p) inside the domain \mathcal{R} the linear feedback control $v_{\mathcal{R}}(\alpha, p)$ defined by

$$v_{\mathcal{R}}(\alpha, p) = (B_p(\tau_0) \quad A_p(\tau_0)B_p(\tau_0))^{-1} \left[\begin{pmatrix} \hat{\alpha}(h) \\ \hat{p}(h) \end{pmatrix} - A_p(\tau_0)^2 \begin{pmatrix} \alpha(h) \\ p(h) \end{pmatrix} \right] \Big|_{(2)} \quad (73)$$

is applied. For unconstrained v the feedback (73) is a dead-beat control which achieves convergence of dynamics (71) to $(\hat{\alpha}, \hat{p})$ in two steps. Since in our case v is bounded by (4), the parameters ρ_1 and ρ_2 that define the set $\mathcal{R}(\hat{\alpha}, \hat{p})$ in (72) are chosen such that $\mathcal{R}(\hat{\alpha}, \hat{p})$ be a controlled invariant for dynamics (71) under feedback (73). In conclusion, the discrete-time feedback control for the intake manifold is

$$v(h) = \begin{cases} \begin{cases} +V & \text{if } [(\sigma(\alpha, p) < 0) \vee ((\sigma(\alpha, p) = 0) \wedge (\alpha < \hat{\alpha}))] \wedge (\alpha < 90) \\ -90 \frac{a_\alpha}{b_\alpha} & \text{if } [(\sigma(\alpha, p) < 0) \vee ((\sigma(\alpha, p) = 0) \wedge (\alpha < \hat{\alpha}))] \wedge (\alpha = 90) \\ -V & \text{if } [(\sigma(\alpha, p) > 0) \vee ((\sigma(\alpha, p) = 0) \wedge (\alpha > \hat{\alpha}))] \wedge (\alpha > 0) \\ 0 & \text{if } [(\sigma(\alpha, p) > 0) \vee ((\sigma(\alpha, p) = 0) \wedge (\alpha > \hat{\alpha}))] \wedge (\alpha = 0) \end{cases} & \text{if } (\alpha, p) \notin \mathcal{R}(\hat{\alpha}, \hat{p}) \\ v_{\mathcal{R}}(\alpha, p) & \text{if } (\alpha, p) \in \mathcal{R}(\hat{\alpha}, \hat{p}) \end{cases} \quad (74)$$

with $v_{\mathcal{R}}(\alpha, p)$ as in (73).

3.3.2 Outer loop: torque generation control

In order to be able to apply the feedback control loop for the torque generation developed in Section 3.2 to the engine as described by the hybrid model presented in Section 2.5, the following points need to be addressed:

1. in the optimal control Problem (3.2.1), the discrete-time model of the system has been assumed to evolve with a fixed sampling frequency of period equal to τ , i.e. the engine is supposed to run at fixed crankshaft velocity. Indeed, only under such hypothesis the reference signal $\hat{T}(k)$ in (49) is actually a ramp signal;

2. in the expression of the optimal control (65), the bounds on the desired manifold pressure \tilde{p} , \tilde{p}_{min} and \tilde{p}_{max} are supposed to be fixed and known, while in the overall model they depend on the intake manifold dynamics;
3. the engine inputs $v(h)$ and $\gamma(k)$ are asynchronous: the former evolves at a fixed sampling frequency $1/\tau_0$, while the latter is synchronous with the dead centers.
4. the feedback law needs to be generalized to the case where a generic (non-ramp) reference torque signal is applied.

At each time t_k of the sequence of dead centers times $\{t_k\}$, the torque generation feedback law (65) gives the current value of the equivalence ratio $\gamma(k)$ for fuel injection and the current value of desired intake manifold pressure $\tilde{p}(k)$ for the inner intake manifold control loop. To include reference torque signals \hat{T} which are different from the ramp-signal, at each t_k the given signal is locally approximated by the tangent line by setting in (65)

$$\hat{T}(k+2) = \hat{T}(k) + 2m_{\hat{T}}(k) \tilde{\tau}(k) \quad (75)$$

where $\tilde{\tau}(k) = 30/n(t_k)$ is the current estimate of the dead center period (obtained from the crankshaft velocity measurement) and

$$m_{\hat{T}}(k) = \frac{\hat{T}(k) - \hat{T}(k-1)}{\tau(k-1)} \quad (76)$$

with $\tau(k-1)$ the measured time between the current and the previous dead center. In the following section, the robustness with respect to the evolution of the crankshaft velocity of the feedback control (65) with value of the next dead center time τ replaced by the estimate $\tilde{\tau}$, will be analyzed in depth.

Moreover, the implementation of the control (65) in the outer control loop requires also estimates of the bounds \tilde{p}_{min} and \tilde{p}_{max} , which define the feasible range for desired intake manifold pressure. At each dead center the following estimates are used

$$\begin{aligned} \tilde{p}_{min}(k) &= A_p(\tilde{\tau}(k)) \begin{pmatrix} \alpha(k) \\ p(k) \end{pmatrix} - B_p(\tilde{\tau}(k))V \Big|_{(2)} \\ \tilde{p}_{max}(k) &= A_p(\tilde{\tau}(k)) \begin{pmatrix} \alpha(k) \\ p(k) \end{pmatrix} + B_p(\tilde{\tau}(k))V \Big|_{(2)} \end{aligned} \quad (77)$$

where $A_p(\cdot)$ and $B_p(\cdot)$ are given by (41).

At each dead center time t_k the feedback outer-loop control (65) returns the value $\tilde{p}(k)$ of the desired manifold pressure to be used by the inner-loop intake manifold control (74). Feedback (74) is based on the reference trajectory for the intake manifold state $(\hat{\alpha}, \hat{p})$ given by (25) and (24), which has to be derived from the values $\tilde{p}(k)$. The asynchronousness of the two control loops is solved by interpolating the values of the sequence $\tilde{p}(k)$, generated at dead-center times $\{t_k\}$, on the fixed time base $\{t_h\}$ of the intake manifold control.

Given a time t_k let $\bar{h}(k) = \operatorname{argmin}_h (t_h > t_k)$. For all h with $t_h \in [t_{\bar{h}(k)}, t_{\bar{h}(k+1)})$, the reference trajectory $(\hat{\alpha}, \hat{p})$ is defined according to (25) and (24) by choosing

$$m_p = m_{\tilde{p}}(k) = \frac{\tilde{p}(k) - \tilde{p}(k-1)}{\tau(k-1)} \quad (78)$$

$$n_p = n_{\tilde{p}}(k) = \tilde{p}(k) \quad (79)$$

In conclusion, the hybrid tracking feedback control is summarized below.

Fuel injection control — running at dead-center times $\{t_k\}$
 compute $\tilde{T}(k+2)$ according to (75)
 compute $\tilde{p}_{min}, \tilde{p}_{max}$ according to (77) (80)
 compute $\tilde{p}(k)$ and set $\gamma(k)$ according to (65)
 compute $m_{\tilde{p}}(k), n_{\tilde{p}}(k)$ according to (78–79)

Intake manifold control — running at fixed sampling $\{t_h\}$
 compute $\sigma(\alpha, p)$ according to (44) with $m_p = m_{\tilde{p}}(k), n_p = n_{\tilde{p}}(k)$ (81)
 set $v(h)$ according to (74)

4 Analysis of the robustness of the torque tracking control

We report here the results on the analysis of the robustness properties of the hybrid feedbacks (80) and (81) when applied to the hybrid engine model presented in Section 2. Such analysis is developed through a sequence of incremental steps. Starting from an abstraction of the hybrid engine model, at each step the model is refined until its complete description is achieved.

The robustness analysis is developed through the following steps:

- R.1 fixed crankshaft velocity and ramp-signal reference torque;
- R.2 fixed crankshaft velocity and generic reference torque;
- R.3 hybrid plant model and generic reference torque.

4.1 R.1: fixed crankshaft velocity and ramp-signal reference torque

We start the study of the robustness properties of the proposed hybrid feedback considering a relaxed hybrid model of the engine where

- the crankshaft speed is supposed to be constant, i.e. $n(t) = 30/\tau$, and
- the reference torque signal \hat{T} is a ramp-signal of type (49).

We will show that:

Proposition 4.1.1 *If the reference signal \hat{T} satisfies the hypothesis of Lemma 3.2.3, where \tilde{p}_{min} and \tilde{p}_{max} are given by (77), and if*

$$Q \leq \min \left\{ \left| \frac{\tilde{p}_{max} - \hat{T}(k+2)}{l(k+1)} \right|, \left| \frac{\tilde{p}_{min} - \hat{T}(k+2)}{l(k+1)} \right| \right\} \quad \text{and} \quad Q \in (0, 1] \quad (82)$$

then

- $T(k) = \hat{T}(k)$, for all k greater than some finite $K > 0$, and
- $\lim_{k \rightarrow \infty} l(k) = 0$.

If the manifold pressure is affected by a multiplicative disturbance $\varepsilon_M(k)$ and an additive disturbance $\varepsilon_A(k)$, that is

$$p(k) = \tilde{p}(k)\varepsilon_M(k) + \varepsilon_A(k), \quad (83)$$

with $\varepsilon_M(k)$ and $\varepsilon_A(k)$ bounded as

$$|\varepsilon_M(k) - 1| \leq d_M < 1 \quad \text{and} \quad |\varepsilon_A(k)| \leq d_A. \quad (84)$$

then $\lim_{k \rightarrow \infty} l(k) = L < \infty$.

Proof. Consider first the convergence of $T(k)$ to $\hat{T}(k)$. If, given some \bar{k} , we have

$$p(k+1) \in \left[\frac{\hat{T}(k+2)}{Gc_p\gamma_{max}}, \frac{\hat{T}(k+2)}{Gc_p\gamma_{min}} \right] \quad \forall k > \bar{k} \quad (85)$$

$$p(k+1) = \tilde{p}(k+1) \quad \forall k > \bar{k} \quad (86)$$

then the outer control loop (65) can set a proper value for $\gamma(k)$ so that $T(k+2) = \hat{T}(k+2)$. The existence of a value \bar{k} for which (85) and (86) hold is guaranteed by Lemma 3.2.3. In fact, (85) trivially follows from (67), while (86) is implied by (82). Hence,

$$T(k) = \hat{T}(k) \quad \text{for any } k > K = \bar{k} + 2.$$

Since (86) holds, then by Lemma (3.2.3), $\lim_{k \rightarrow \infty} l(k) = 0$ provided that $Q \in (0, 1]$.

Let the manifold pressure $p(k)$ be affected by disturbances as in (83). By (49), we have $l(k+2) = l(k+1) + c_p p(k)(1 - \gamma(k))$. Moreover, since $T(k) = \hat{T}(k)$, by (65) and (83),

$$l(k+2) = l(k+1) + c_p(\tilde{p}(k)\varepsilon_M(k) + \varepsilon_A(k)) - \frac{\hat{T}(k+2)}{G}$$

and, by (65) and (67),

$$l(k+2) = l(k+1)(1 - Q\varepsilon_M(k)) + \frac{\hat{T}(k+2)}{G}(\varepsilon_M(k) - 1) + c_p\varepsilon_A(k),$$

which gives

$$l(k) = l(\bar{k}+2)(1 - Q\varepsilon_M(\bar{k}+k+1-i))^k + \sum_{i=0}^{k-\bar{k}-2} (1 - Q\varepsilon_M(\bar{k}+k+1-i))^i \left(\frac{\hat{T}(\bar{k}+k+3-i)(\varepsilon_M(\bar{k}+k+1-i) - 1) + c_p\varepsilon_A(\bar{k}+k+1-i)}{G(1 - Q\varepsilon_M(\bar{k}+k+1-i))} \right). \quad (87)$$

Then

$$|l(k)| \leq M \sum_{i=0}^{k-\bar{k}-2} |1 - Q\varepsilon_M(\bar{k} + k + 1 - i)|^k \leq M \sum_{i=0}^{\infty} |1 - Q(1 - d_M)|^k$$

where $M = \frac{(\max_i \hat{T}(i))d_M + c_p d_A}{G(1 - Qd_M)}$. Hence, since for any $Q \in (0, 1]$ and $d_M \in (0, 1)$, $1 - Q(1 - d_M) < 1$ then the upper bounding series converges and

$$\lim_{k \rightarrow \infty} |l(k)| \leq \sum_{i=0}^{\infty} M |1 - Q\varepsilon_M(\bar{k} + k + 1 - i)|^k \leq \frac{M}{Q(1 - d_M)} = L$$

The closest $Q(1 - d_M)$ is to 1, the faster is the convergence of $l(k)$ and the lowest upper bound L . \square

Note that, if Q is small the upper bounds d_A and d_M are small since the reference air $\tilde{p}(k)$ is smooth and can be easily tracked by $p(k)$.

4.2 R.2: fixed crankshaft velocity and generic reference torque

When a generic (non-ramp) reference torque signal $\hat{T}(t)$ is required to be tracked, the hybrid feedback control (80) computes, at each dead point, the next value of the requested torque by approximating locally the reference signal with tangent according to (75).

If the crankshaft velocity is fixed at $30/\tau$ then, at a given dead center time t_k , the hybrid feedback control (80) and (81) produces a torque $T(t_k)$ that exactly matches the value of the ramp signal starting at time t_{k-2} with value $\hat{T}(t_{k-2})$.

If the second derivative with respect to time of the reference torque signal $\hat{T}(t)$ is bounded by M'' , then at each dead center, the error between the reference signal $\hat{T}(t_k)$ and the produced torque is upper bounded by

$$|T(t_k) - \hat{T}(t_k)| \leq 4M''\tau^2 \quad (88)$$

In the intake manifold inner-loop control, the discontinuities due to a non-ramp torque signal are added to those due to the modulation of $\tilde{p}(h)$ introduced by the equivalence ratio $\gamma(k)$ modulation. Hence, non-ramp reference signals do not qualitatively change the behavior of the inner loop.

4.3 R.3: hybrid plant model and generic reference torque

Consider now the case where the hybrid feedback control (80) and (81) is applied to the hybrid engine model described in Section 2. In such model the sequence of dead center times is not equally spaced as supposed in the previous two sections.

Let $\tau_d(k)$ denote the difference between the time $\tau(k)$ between the next and the current dead center and its estimated value $\tilde{\tau}(k)$, i.e.

$$\tau_d(k) = \tau(k) - \tilde{\tau}(k)$$

and let $\tau_d(k) \leq \tau_M$ for some τ_M .

By (49) and (76), $T(k+2) = G[\tilde{p}(k+1) + m_{\tilde{p}}(k+1)\tau_d(k+1)]\gamma(k)$. Assuming that feedback control has locked the reference signal $\hat{T}(k)$ and replacing according to (65) $\gamma(k)$ with $\frac{\hat{T}(k+2)}{Gc_p\tilde{p}(k+1)}$, we have

$$T(k+2) = \hat{T}(k+2) + \left(m_{\hat{T}}(k) + G \frac{m_p(k+1)}{\tilde{p}(k+1)} \right) \tau_d(k+1) + m_{\hat{T}}(k)\tau_d(k+2).$$

Hence, the torque produced is composed of: the linear approximation of the reference signal and a disturbance due to the terms multiplying $m_{\hat{T}}(k)$ and $m_{\tilde{p}}(k+1)$. The first term represents the error on the linear interpolation of the torque and is numerically larger than the second one, that is due to errors on manifold pressure measurement time.

Further, recall that, the value $\hat{T}(k+2)$ obtained by the tangent approximation of the torque reference signal, is affected by an error which can be upper bounded as in (88)

Variable $l(k)$ is affected only by the error on the manifold pressure measurement time:

$$l(k+2) = l(k+1)(1-Q) + m_{\tilde{p}}(k+1)(1-\gamma(k))\tau_d(k)$$

Since $(1-\gamma(k))$ and $m_{\tilde{p}}(k+1)$ are bounded, then for any $Q \in (0, 1)$

$$\lim_{k \rightarrow \infty} |l(k)| < L$$

where L is proportional to $\frac{1}{1-Q}$ and τ_M .

5 Simulations

In Figure 6 a minimum-time trajectory of the intake manifold dynamics (28) to a ramp-signal reference pressure as in (24), obtained applying the optimal control (47) developed in Section 3.1, is reported. According to the theoretical study, the optimal control v has only one switching before approaching the reference signal.

Figures 7,8 and 9 report the results of the simulation of the hybrid engine model described in Section 2 under the hybrid tracking-control feedback (80) and (81) for ramp and sinusoidal reference torque signals.

In Figure 7 a ramp-signal reference-torque is applied. The control action is composed of two subsequent parts:

- first, overloading the catalytic converter, the control signals attempt to achieve the reference torque by using an equivalence ratio γ greater than the stoichiometric value 1;
- then, keeping the torque locked on the reference signal, the control balances the catalytic converter by driving the manifold pressure to values that both guarantee torque tracking and, at the same time, produce lean mixture until the catalytic converter is recovered.

The catalytic converter is loaded until the intake manifold dynamics approaches the manifold pressure reference signal; then its recovery begins and the torque approaches the reference signal. At each dead center, a new reference signal is provided to the intake manifold inner-loop. Hence, the errors on the estimation of the next dead center time produce a noise on

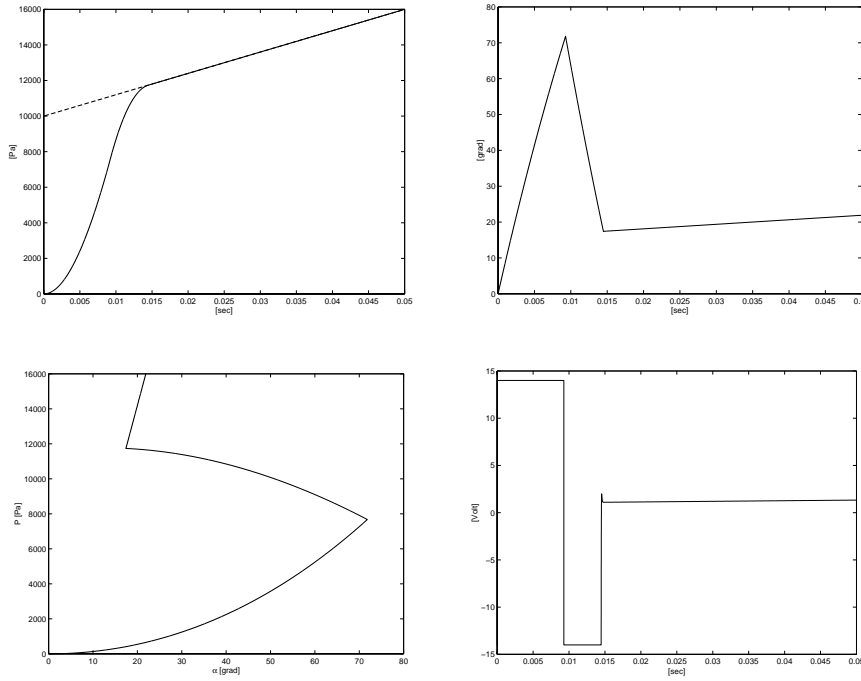


Figure 6: Simulation of intake manifold under continuous-time feedback control low (47). Top-Left: Intake manifold pressure $p(t)$; Top-Right: Throttle valve angle $\alpha(t)$; Down-Left: State-space trajectory $\alpha(t), p(t)$; Down-Right: Input control $v(t)$.

the reference manifold pressure signal $\tilde{p}(h)$. To reduce the negative effects of such noise in the intake manifold inner-loop, the signal $\tilde{p}(h)$ is filtered through a one-order low-pass filter. The control $v(h)$ changes according to the reference manifold pressure $\tilde{p}(h)$ so, the discontinuities of $\tilde{p}(h)$ which are produced at each dead center appear also on the input signal $v(h)$. Such discontinuities decrease when the catalytic converter is balanced because, in this case, $\tilde{p}(h)$ depend only on the torque reference signal which is smooth.

In Figure 8 the reference-signal is a sinusoid-signal, whose peak value can be produced by the engine with a stoichiometric mixture. The closed-loop system behavior is similar to that of the previous case, except for the fact that the discontinuities of $v(h)$ do not decrease since the requested torque does not produce a ramp-signal desired manifold pressure.

Finally, in Figure 9 the reference-signal is a sinusoid-signal, whose peak value cannot be produced with stoichiometric mixture. At first, the control law attempts to achieve the requested torque, then it tries to recover the catalytic converter until the torque reference become too high to be produced. The catalytic converter, overloaded to achieve the torque, is kept unbalanced to remain close to the desired torque, but, when it reaches its physical constraint, it forces to use either stoichiometric or lean mixture. This phenomenon generates a discontinuity on the produced torque that is clamped on the reference value until the catalytic converter reaches its constraints, then it jumps to the maximal torque generatable at stoichiometric. The recovery of catalytic converter begins when the reference torque signal becomes small enough.

Appendix

Proof of Lemma 3.2.1. Let us first show that for a given $u(k)$, (64) \Rightarrow (63). If $\gamma(k)$ and $\tilde{p}(k)$

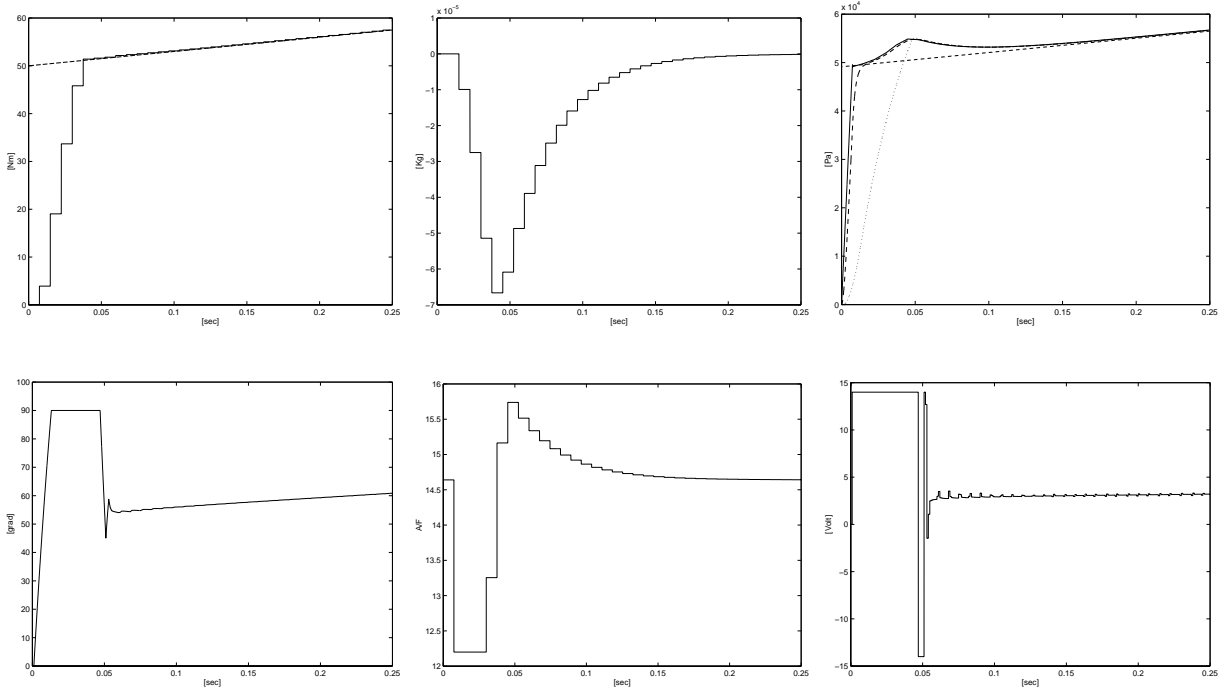


Figure 7: Simulation of hybrid model engine under control (80,81), excited by a ramp-signal reference. Top-Left: Torque produced and torque reference signal; Top-Center: catalytic converter status $l(k)$; Top-Right: Intake manifold pressure $p(t)$; Down-Left: Throttle valve angle $\alpha(t)$; Down-Center: Input mix Air-Fuel $\gamma(k)$; Down-Right: Input control $v(t)$.

are as in (64), then $\gamma(k) \in [\gamma_{min}, \gamma_{max}]$ and $\in [\tilde{p}_{min}, \tilde{p}_{max}]$. Consider the following cases:

- let $\gamma(k) \in (\gamma_{min}, \gamma_{max})$ and $\tilde{p}(k) \in [\gamma_{min}, \gamma_{max}]$. If $\bar{\gamma}(k) = \gamma(k) = \frac{\hat{T}(k+2)}{G_{c_p} \tilde{p}(k)}$ then $u(k) = \gamma(k) \tilde{p}(k) = \frac{\hat{T}(k+2)}{G_{c_p}} \in (\tilde{p}_{min} \gamma_{min}, \tilde{p}_{max} \gamma_{max})$.
- let $\tilde{p}(k) \in (\gamma_{min}, \gamma_{max})$ and $\gamma(k) \in [\gamma_{min}, \gamma_{max}]$. Since $\tilde{p}(k) = \frac{\hat{T}(k+2)}{G_{c_p} \bar{\gamma}(k)}$, then choosing $\bar{\gamma}(k) = \gamma(k)$, we have $u(k) = \gamma(k) \tilde{p}(k) = \frac{\hat{T}(k+2)}{G_{c_p}} \in (\tilde{p}_{min} \gamma_{min}, \tilde{p}_{max} \gamma_{max})$.
- let $\tilde{p}(k) = \tilde{p}_{max}$ and $\gamma(k) = \gamma_{max}$. By (64) $\frac{\hat{T}(k+2)}{G_{c_p} \tilde{p}_{max}(k)} \geq \gamma_{max}$ and, choosing $\bar{\gamma} = \gamma_{max}$, we have $\frac{\hat{T}(k+2)}{G_{c_p}} \geq u(k) = \tilde{p}_{max} \gamma_{max}$.
- let $\tilde{p}(k) = \tilde{p}_{min}$ and $\gamma(k) = \gamma_{min}$. By (64) $\frac{\hat{T}(k+2)}{G_{c_p} \tilde{p}_{min}} \leq \gamma_{min}$ and, choosing $\bar{\gamma} = \gamma_{min}$, we have $\frac{\hat{T}(k+2)}{G_{c_p}} \leq u(k) = \tilde{p}_{min} \gamma_{min}$.
- let $\tilde{p}(k) = \tilde{p}_{max}$ and $\gamma(k) = \gamma_{min}$. By (64) $\tilde{p}_{max} \leq \frac{\hat{T}(k+2)}{G_{c_p} \bar{\gamma}(k)} \leq \frac{\hat{T}(k+2)}{G_{c_p} \gamma_{min}} \leq \tilde{p}_{max}$ then choosing $\bar{\gamma} = \frac{\hat{T}(k+2)}{G_{c_p} \tilde{p}_{max}}$, $u(k) = \gamma_{min} \tilde{p}_{max} = \frac{\hat{T}(k+1)}{G_{c_p}} \in (\tilde{p}_{min} \gamma_{min}, \tilde{p}_{max} \gamma_{max})$
- let $\tilde{p}(k) = \tilde{p}_{min}$ and $\gamma = \gamma_{max}(k)$. By (64) $\tilde{p}_{min} \geq \frac{\hat{T}(k+2)}{G_{c_p} \bar{\gamma}(k)} \geq \frac{\hat{T}(k+2)}{G_{c_p} \gamma_{max}} \geq \tilde{p}_{min}$, then choosing $\bar{\gamma} = \frac{\hat{T}(k+2)}{G_{c_p} \tilde{p}_{min}}$, we have $u(k) = \gamma_{max} \tilde{p}_{min} = \frac{\hat{T}(k+1)}{G_{c_p}} \in (\tilde{p}_{min} \gamma_{min}, \tilde{p}_{max} \gamma_{max})$.

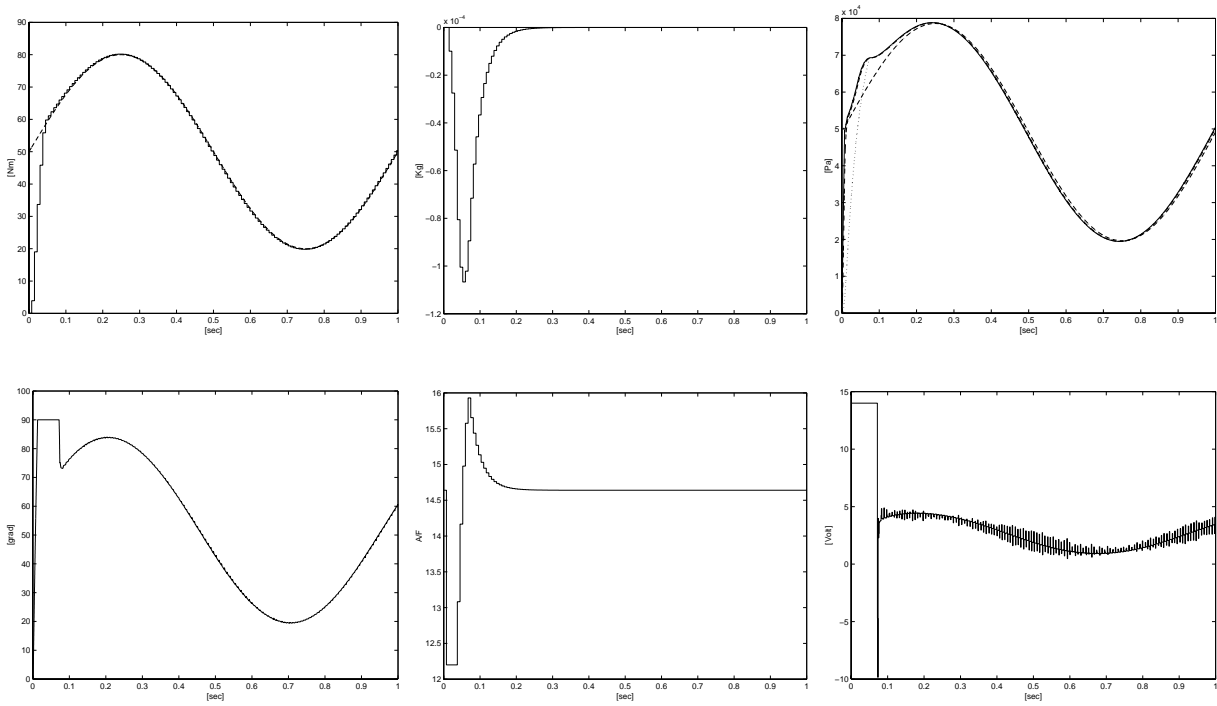


Figure 8: Simulation of hybrid model engine under control (80,81), excited by a short excursion sinusoid-signal reference. Top-Left: Torque produced and torque reference signal; Top-Center: catalytic converter status $l(k)$; Top-Right: Intake manifold pressure $p(t)$; Down-Left: Throttle valve angle $\alpha(t)$; Down-Center: Input mix Air-Fuel $\gamma(k)$; Down-Right: Input control $v(t)$.

Implication (63) \Rightarrow (64) is trivial. Indeed, if for some $u(k)$ (63) yields then any $\gamma(k)$ and $\tilde{p}(k)$ that satisfy $\gamma(k)\tilde{p}(k) = u(k)$ can be written as in (64) for some $\tilde{\gamma} \in [\gamma_{min}, \gamma_{max}]$. \square

Proof of Lemma 3.2.2. Three cases are in order:

1. Let $\tilde{\gamma} > 1$. We have $\tilde{\gamma} > 1 > \gamma_{min}$. Further, assume that $\tilde{\gamma} < \gamma_{max}$. Since $l(k) + c_p p(k)(1 - \gamma^C(k)) = l(k+1)$, then by (67) $\tilde{\gamma} = \frac{\hat{T}(k+2)}{\hat{T}(k+2) - QG l(k+1)} > 1$. Hence, since $QG > 0$ then $l(k+1) > 0$. The same holds when $\tilde{\gamma} = \gamma_{max}$. By (68),

$$\begin{aligned} \gamma_{max} &\leq 1 - \frac{l_{min}}{c_p \tilde{p}_{max}} \leq 1 - \frac{l_{min}}{c_p \tilde{p}_{max}} + \frac{l(k+1)}{c_p \tilde{p}_{max}} \leq 1 - \frac{l_{min}}{c_p \tilde{p}(k)} + \frac{l(k+1)}{c_p \tilde{p}(k)} = \gamma_{max} \\ &\leq 1 + \frac{l(k) + c_p p(k)(1 - \gamma^C(k)) - l_{min}}{c_p \tilde{p}(k)} \end{aligned}$$

Then, by (66) $\hat{\gamma}_{max} = \gamma_{max}$.

2. Let $\tilde{\gamma} = 1$. We have $l(k+1) = 0$ and by (66) $\hat{\gamma}_{max} = \gamma_{max}$ and $\hat{\gamma}_{min} = \gamma_{min}$.

3. Let $\tilde{\gamma} < 1$. Analogously to case 1., we have $\tilde{\gamma} < 1 < \gamma_{max}$. Further, by (67) $l(k+1) < 0$ and

$$\begin{aligned} \gamma_{min} &\geq 1 - \frac{l_{max}}{c_p \tilde{p}_{min}} \geq 1 - \frac{l_{max}}{c_p \tilde{p}_{min}} + \frac{l(k+1)}{c_p \tilde{p}_{min}} \geq 1 - \frac{l_{max}}{c_p \tilde{p}(k)} + \frac{l(k+1)}{c_p \tilde{p}(k)} = \gamma_{min} \\ &\geq 1 + \frac{l(k) + c_p p(k)(1 - \gamma^C(k)) - l_{max}}{c_p \tilde{p}(k)} \end{aligned}$$

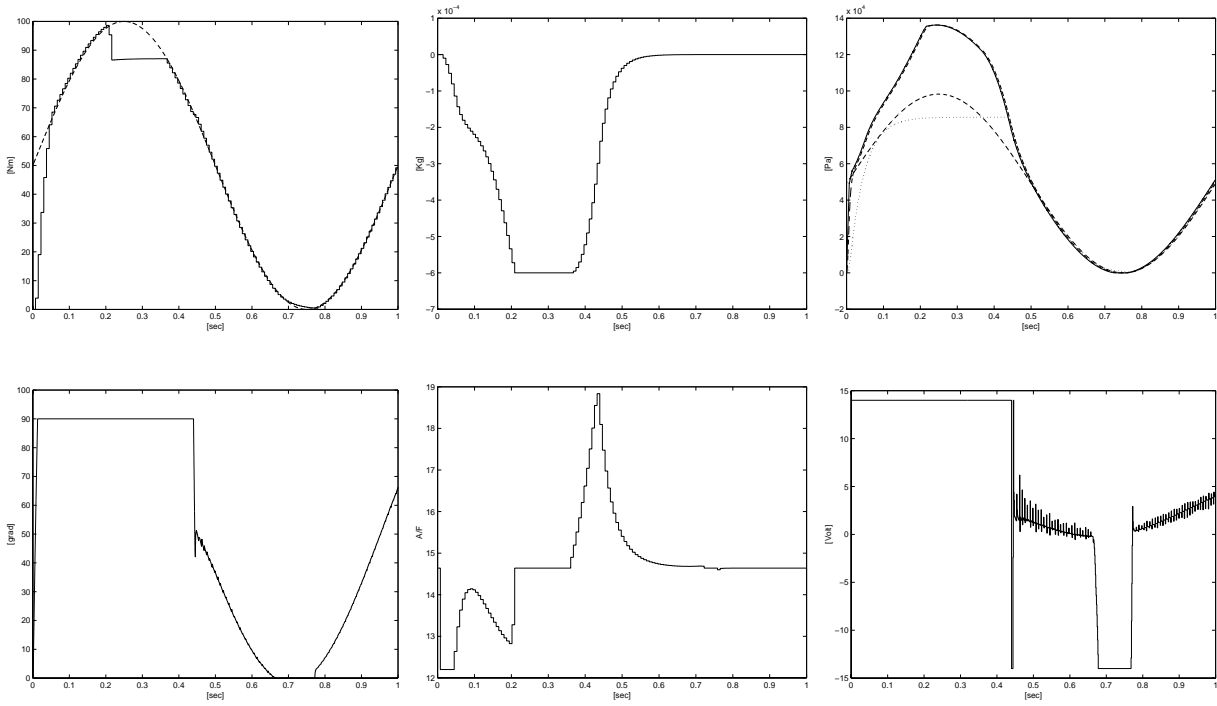


Figure 9: Simulation of hybrid model engine under control (80,81), excited by a wide excursion sinusoid-signal reference. Top-Left: Torque produced and torque reference signal; Top-Center: catalytic converter status $l(k)$; Top-Right: Intake manifold pressure $p(t)$; Down-Left: Throttle valve angle $\alpha(t)$; Down-Center: Input mix Air-Fuel $\gamma(k)$; Down-Right: Input control $v(t)$.

Then, by (66) $\hat{\gamma}_{min} = \gamma_{min}$.

Summarizing: if $\bar{\gamma} \in [1, \gamma_{max}]$ then, $\bar{\gamma} \in [1, \hat{\gamma}_{max}]$, while if $\bar{\gamma} \in [\gamma_{min}, 1]$ then $\bar{\gamma} \in [\hat{\gamma}_{min}, 1]$. \square

Proof of Lemma 3.2.3. Let $\bar{\gamma}(k) = (\frac{\hat{T}(k+2)}{\hat{T}(k+2) - GQl(k+1)})$ and consider the following cases:

1. Let $\frac{\hat{T}(k+2)}{Gc_p\bar{\gamma}(k)} > \tilde{p}_{max}$. By (69), it follows $\bar{\gamma}(k) < \frac{\hat{T}(k+2)}{Gc_p\tilde{p}_{max}} < 1$. Further, since by (65) $\gamma(k) < 1 < \hat{\gamma}_{max}$ and by (67) $\bar{\gamma}(k) < 1 < \hat{\gamma}_{max}$, then

$$\bar{\bar{\gamma}}(k) \leq \bar{\gamma}(k) \leq \frac{\hat{T}(k+2)}{Gc_p\tilde{p}_{max}} \leq \gamma(k) < 1 \quad (89)$$

Then, by (49),

$$l(k+1) > l(k+2) = l(k+1) + c_p\tilde{p}(k)(1 - \gamma(k)) \geq l(k+1) + c_p\tilde{p}(k)(1 - \bar{\bar{\gamma}}(k)) \geq l(k+1)(1 - Q)$$

where the definition of $\bar{\bar{\gamma}}(k)$ has been used. Further, since by (67), $\bar{\bar{\gamma}}(k) < 1$ only if $l(k+1) > 0$, then

$$l(k+1) > l(k+2) \geq l(k+1)(1 - Q) > 0$$

2. Let $\frac{\hat{T}(k+2)}{Gc_p\bar{\gamma}(k)} < \tilde{p}_{min}$. By (69), it follows $\bar{\gamma}(k) > \frac{\hat{T}(k+2)}{Gc_p\tilde{p}_{max}} > 1$. Further, since by (65) $\gamma(k) > 1 > \hat{\gamma}_{min}$ and by (67) $\bar{\gamma}(k) > 1 > \hat{\gamma}_{min}$, then

$$\bar{\bar{\gamma}}(k) \geq \bar{\gamma}(k) \geq \frac{\hat{T}(k+2)}{Gc_p\tilde{p}_{max}} \geq \gamma(k) > 1 \quad (90)$$

Then, by (49),

$$l(k+1) < l(k+2) = l(k+1) + c_p \tilde{p}(k)(1 - \gamma(k)) \leq l(k+1) + c_p \tilde{p}(k)(1 - \bar{\gamma}(k)) \leq l(k+1)(1 - Q)$$

where the definition of $\bar{\gamma}(k)$ has been used. Further, since by (67), $\bar{\gamma}(k) > 1$ only if $l(k+1) < 0$, then

$$l(k+1) < l(k+2) \leq l(k+1)(1 - Q) < 0$$

3. Let $\tilde{p}_{min} \leq \frac{\hat{T}(k+2)}{G c_p \bar{\gamma}(k)} \leq \tilde{p}_{max}$. By (65), we have $\gamma(k) = \bar{\gamma}(k)$. Three cases are in order:

- Let $\gamma_{min} < \bar{\gamma}(k) < \gamma_{max}$. Then, by (67), $\gamma(k) = \bar{\gamma}(k)$ and $l(k+2) = (1 - Q)l(k+1)$ which is stable for $Q \in (0, 1]$.

- Let $\bar{\gamma}(k) \geq \gamma_{max}$. Since, by (67), $\bar{\gamma}(k) \geq \gamma(k)$ then by (49),

$$l(k+1) > l(k+2) = l(k+1) + c_p \tilde{p}(k)(1 - \gamma(k)) \geq l(k+1) + c_p \tilde{p}(k)(1 - \bar{\gamma}(k)) \geq (1 - Q)l(k+1) > 0$$

where the definition of $\bar{\gamma}(k)$ has been used.

- Let $\bar{\gamma}(k) \leq \gamma_{min}$. Since, by (67), $\bar{\gamma}(k) \leq \gamma(k)$ then by (49),

$$l(k+1) < l(k+2) = l(k+1) + c_p \tilde{p}(k)(1 - \gamma(k)) \leq l(k+1) + c_p \tilde{p}(k)(1 - \bar{\gamma}(k)) \leq (1 - Q)l(k+1) < 0$$

where the definition of $\bar{\gamma}(k)$ has been used.

Summarizing we have

$$0 \leq (1 - Q)|l(k+1)| \leq |l(k+2)| < |l(k+1)|$$

as in (70). \square

References

- [1] M. ABATE AND V. DI NUNZIO, *Idle speed control using optimal regulation*, Tech. Rep. 905008, SAE, 1990.
- [2] R. ALUR AND T. A. HENZINGER, eds., *Hybrid Systems III*, no. 1066 in Lecture Notes in Computer Science, Springer-Verlag, 1996.
- [3] M. ANTONIOTTI, A. BALLUCHI, L. BENVENUTI, A. FERRARI, C. PINELLO, A. L. SANGIOVANNI-VINCENTELLI, R. FLORA, W. NESCI, C. ROSSI, G. SERRA, AND M. TABARO, *A top-down constraints-driven design methodology for powertrain control system*, in Proc. GPC98, Global Powertrain Congress, vol. Emissions, Testing and Controls, Detroit, Michigan, USA, October 1998, pp. 74–84.
- [4] P. ANTSAKLIS, W. KOHN, M. LEMMON, A. NERODE, AND S. SASTRY, eds., *Hybrid Systems V*, no. 1567 in Lecture Notes in Computer Science, Springer-Verlag, 1999.

- [5] P. ANTSAKLIS, A. NERODE, W. KOHN, AND S. SASTRY, eds., *Hybrid Systems II: Proceedings of the 1994 Workshop on Hybrid Systems and Autonomous Control*, no. 999 in Lecture Notes in Computer Science, Springer-Verlag, 1995.
- [6] J. K. BALL, R. R. RAINE, AND C. R. STONE, *Combustion analysis and cycle-by-cycle variations in spark ignition engine combustion, part 2: a new parameter for completeness of combustion and its use in modelling cycle-by-cycle variations in combustion*, IMechE Journal of Automobile Engineering, 212 (1998), pp. 507–523.
- [7] A. BALLUCHI, L. BENVENUTI, M. DI BENEDETTO, C. PINELLO, AND A. SANGIOVANNI-VINCENTELLI, *Automotive engine control and hybrid systems: Challenges and opportunities*, Proceedings of the IEEE, (2000).
- [8] A. BALLUCHI, M. D. DI BENEDETTO, C. PINELLO, C. ROSSI, AND A. L. SANGIOVANNI-VINCENTELLI, *Cut-off in engine control: a hybrid system approach*, in Proc. 36th IEEE Conference on Decision and Control, San Diego, California, USA, December 1997, pp. 4720–4725.
- [9] —, *Hybrid control in automotive applications: the cut-off control*, Automatica, 35, Special Issue on Hybrid Systems (1999), pp. 519–535.
- [10] A. BALLUCHI, M. D. DI BENEDETTO, C. PINELLO, AND A. L. SANGIOVANNI-VINCENTELLI, *A hybrid approach to the fast positive force transient tracking problem in automotive engine control*, in Proc. 37th IEEE Conference on Decision and Control, Tampa, Florida, USA, December 1998, pp. 3226–3231.
- [11] M. BRANICKY, *Multiple lyapunov functions and other analysis tools for switched and hybrid systems*, IEEE Trans. on Aut. Contr., 43 (1998), pp. 475–482.
- [12] A. E. BRYSON AND Y.-C. HO, *Applied optimal control, optimization, estimation, and control*, John Wiley and Sons, Inc., New York, N.Y., 1975.
- [13] K. R. BUTTS, N. SIVASHANKAR, AND J. SUN, *Application of ℓ_1 optimal control to the engine idle speed control problem*, IEEE Trans. on Control Systems Technology, 7 (1999), pp. 258–270.
- [14] S. B. CHOI AND J. K. HEDRICK, *An observer-based controller design method for improving air/fuel characteristics of spark ignition engines*, IEEE Trans. on Control Systems Technology, 6 (1998), pp. 325–334.
- [15] A. CHOW AND M. L. WYSYNSKI, *Thermodynamic modelling of complete engine systems - a review*, IMechE Journal of Automobile Engineering, 213 (1999), pp. 403–415.
- [16] A. CHUTINAN AND B. KROGH, *Verification of polyhedral-invariant hybrid automata using polygonal flow pipe approximations*, in Hybrid Systems: Computation and Control, LNCS, Springer-Verlag, London, 1999.
- [17] J. A. COOK AND B. K. POWEL, *Modeling of an internal combustion engine for control analysis*, IEEE Control Systems, (1988), pp. 20–25.

- [18] T. DANG AND O. MALER, *Reachability analysis via face lifting*, in HSCC 98: Hybrid Systems—Computation and Control, T. A. Henzinger and S. Sastry, eds., Lecture Notes in Computer Science 1386, Springer-Verlag, 1998, pp. 96–109.
- [19] J. H. *et al.*, *Experimental and theoretical analysis of flame development and misfire phenomena in a spark-ignition engine*, Tech. Rep. 920415, SAE, 1992.
- [20] A. E.-D. M. FOR PREDICTING TRANSIENT FUEL ECONOMY AND C.-O. E. EMISSIONS, *J.d. murrell and g.m. lewis and d.n. assanis*, Tech. Rep. 971838, SAE, 1997.
- [21] M. L. FRANKLIN AND T. E. MURPHY, *A study of knock and power loss in the automotive spark ignition engine*, Tech. Rep. 890161, SAE, 1989.
- [22] R. GROSSMAN, A. NERODE, A. RAVN, AND H. RISCHER, eds., *Hybrid Systems*, no. 736 in Lecture Notes in Computer Science, Springer-Verlag, 1993.
- [23] Y. Y. HAM, K. M. CHUM, J. H. LEE, AND K. S. CHANG, *Spark-ignition engine knock control and threshold value determination*, Tech. Rep. 960496, SAE, 1996.
- [24] E. HENDRICKS, A. CHEVALIER, M. JENSEN, AND T. VESTERHOLM, *Event based engine control: Practical problems and solutions*, Tech. Rep. No. 950008, SAE, 1995.
- [25] E. HENDRICKS AND S. C. SORENSON, *Mean value modelling of spark ignition engines*, Tech. Rep. No. 900616, SAE, 1990.
- [26] E. HENDRICKS AND T. VESTERHOLM, *The analysis of mean value SI engine models*, Tech. Rep. No. 920682, SAE, 1992.
- [27] T. HENZINGER AND P.-H. HO, *HYTECH: The Cornell Hybrid Technology Tool*, in Hybrid Systems II, P. Antsaklis, A. Nerode, W. Kohn, and S. Sastry, eds., Lecture Notes in Computer Science 999, Springer-Verlag, 1995, pp. 265–293.
- [28] T. A. HENZINGER, P.-H. HO, AND H. WONG-TOI, *HYTECH: A model checker for hybrid systems*, Software Tools for Technology Transfer, 1 (1997), pp. 110–122.
- [29] T. A. HENZINGER AND S. SASTRY, eds., *Hybrid Systems: Computation and Control*, no. 1386 in Lecture Notes in Computer Science, Springer-Verlag, 1998. Proc. of the First International Workshop, HSCC’98.
- [30] ———, eds., *Hybrid Systems: Computation and Control*, no. 1569 in Lecture Notes in Computer Science, Springer-Verlag, 1999. Proc. of the Second International Workshop, HSCC’99.
- [31] J. B. HEYWOOD, *Internal Combustion Engine Fundamental*, Mc-Graw Hill, 1988.
- [32] D. HROVAT, D. COLVIN, AND B. K. POWELL, *Comments on “applications of some new tools to robust stability analysis of spark ignition engine: A case study”*, IEEE Trans. on Control Systems Technology, 6 (1998), pp. 435–436.

- [33] D. HROVAT AND J. SUN, *Models and control methodologies for IC engine idle speed control design*, Control Engineering Practice, 5 (1997).
- [34] G. KÖNIG, R. R. MALY, D. BRADLEY, A. LAU, AND C. SHEPPARD, *Role of exothermic centres on knock initiation and knock damage*, Tech. Rep. 890161, SAE, 1989.
- [35] M. KOURJANSKI AND P. VARAIYA, *Stability of hybrid systems*, in Hybrid Systems III, R. Alur, T. Henzinger, and E. Sontag, eds., Lecture Notes in Computer Science 1066, Springer-Verlag, 1996, pp. 413–423.
- [36] E. LEE AND A. SANGIOVANNI-VINCENTELLI, *A denotational framework for comparing models of computation*, in Proc. International Conference on CAD, Santa Clara, CA, 1996.
- [37] ———, *A framework for comparing models of computation*, IEEE Trans. on Computer-Aided Design of Integrated Circuits and Systems, 17 (1998), pp. 1217–1229.
- [38] K. LEISENRING, B. SAMIMY, AND G. RIZZONI, *IC engine air/fuel ratio feedback control during cold start*, Tech. Rep. 961022, SAE, 1996.
- [39] J. LYGEROS, C. TOMLIN, AND S. SASTRY, *On controller synthesis for nonlinear hybrid systems*, in Proc. of the 37th IEEE Conference on Decision and Control, 1998, pp. 2101–2106.
- [40] O. MALER, ed., *Hybrid and Real-Time Systems*, no. 1201 in Lecture Notes in Computer Science, Springer-Verlag, 1997.
- [41] O. MALER AND S. YOVINE, *Hardware timing verification using KRONOS*, in Proceedings of the IEEE 7th Israeli Conference on Computer Systems and Software Engineering, ICCBSSE'96, Herzliya, Israel, June 1996, IEEE Computer Society Press.
- [42] L. L. MOYNE AND F. MAROTEAUX, *Air-fuel flow modeling applied to the reduction of air-fuel ration excursions during transients on port injected S.I. engines*, Tech. Rep. 970513, SAE, 1997.
- [43] A. NERODE AND W. KOHN, *Models for hybrid systems: Automata, topologies, controllability, observability*, in Hybrid Systems, Lecture Notes in Computer Science 736, Springer-Verlag, 1993, pp. 317–356.
- [44] N. OZDOR, M. DULGER, AND E. SHER, *Cyclic variability in spark ignition engines: a literature survey*, Tech. Rep. 940987, SAE, 1981.
- [45] L. S. PONTRYAGIN, V. G. BOLTYANSKY, R. V. GAMKRELIDZE, AND E. F. MISHCHENKO, *The Mathematical Theory of Optimal Processes*, Wiley, New York, N.Y., 1962.
- [46] S. RICHARD, P. CHEVREL, P. DE LARMINAT, AND B. MARGUERIE, *Polynomial pole placement revisited: Application to active control of a car longitudinal oscillations*, in Proc. 6th IEEE European Control Conference, Karlsruhe, Germany, 1999.
- [47] A. SAITZKOFF, R. RELNMANN, F. MAUSS, AND M. GLAVMO, *In-cylinder pressure measurements using the spark plug as an ionization sensor*, tech. rep., SAE, 970857.

- [48] P. SHAYLER, J. CHICK, N. DARNTON, AND D. EADE, *Generic functions for fuel consumption and engine-out emissions of hc, co and nox of spark-ignition engines*, IMechE Journal of Automobile Engineering, 213 (1999), pp. 365–378.
- [49] D. SHIM, J. PARK, P. P. KHARGONEKAR, AND W. B. RIBBENS, *Reducing automotive engine speed fluctuation at idle*, IEEE Trans. on Control Systems Technology, 4 (1996), pp. 404–410.
- [50] C. R. STONE, *Introduction to Internal Combustion Engines*, Macmillan, London, 1992.
- [51] D.-L. TANG, M.-F. CHANG, AND M. C. SULTAN, *Predictive engine spark timing control*, Tech. Rep. 940973, SAE, 1994.
- [52] S. YURKOVICH AND M. SIMPSON, *Crank-angle domain modeling and control for idle speed*, SAE Journal of Engines, 106 (1997), pp. 34–41.